Development of the Generalised Algorithm for the Modelling of Random Nanoporous Materials

Thesis submitted as a partial fulfilment of requirements

for Master of Technology degree in Materials and Metallurgical Engineering

Navdeep Kumar

Regn. No. 601502002

under the supervision of

Dr. Debabrata Deb

Assistant Professor

School of Physics and Materials Science (SPMS)

Thapar Institute of Engineering and Technology University

Bhadson Road, Patiala, Punjab, Pin -147004, INDIA

DECLARATION

I hereby certify that the work which is being presented in this thesis entitled "**Development of the Generalised Algorithm for the Modelling of Random Nanoporous Materials**" in partial fulfillment of the requirements for the award of Degree of Masters of Technology and submitted in the School of Physics and Materials Science, Thapar University, Patiala, is an authentic record of my own work carried out during the period from January 2017 to June 2017 under the supervision of **Dr. Debabrata Deb**, Assistant Professor, Thapar University Patiala. The matter presented in this thesis has not been submitted by me for the award of any other degree of this or any other university/ institute.

Navdeep Kumar
(Navdeep Kumar)

Date: 15-7-17

CERTIFICATE

It is been certified that the work which is being presented in this thesis entitled "**Development of the Generalised Algorithm for the Modelling of Random Nanoporous Materials**" in partial fulfillment of the requirements for the award of Degree of Masters of Technology and submitted in the School of Physics and Materials Science, Thapar University, Patiala, is an authentic record of the work carried out by **Navdeep Kumar** during the period from January 2017 to June 2017 under the supervision of **Dr. Debabrata Deb**, Assistant Professor, Thapar University Patiala. The matter presented in this thesis has not been submitted for the award of any other degree of this or any other university/ institute.

Thesis Supervisor

(Dr. Debabrata Deb)

Date: 15-7-17

oṁ ajñāna-timirāndhasya jñānāñjana-śalākayā
cakṣur unmīlitam yena tasmai śrī-gurave namaḥ

I offer my respectful obeisances to my teachers,
who have opened my eyes, that were blinded by the darkness of ignorance,
with the torchlight of knowledge.

Acknowledgement

Our personalities are always under the influence of three modes; the mode of goodness, the mode of passion and the mode of ignorance. The mode of goodness is illuminating, the mode of passion materialistic, and the mode of ignorance encourages laziness and inactivity. By the combination of these three modes and the purview of time, we perform certain activities or take decisions. These activities are being carried out from time immemorial and we are suffering or enjoying the fruits of our activities.

The environment we live in, the friends and the peer group we have, everything around us influences the three modes and shapes us. However, we should always keep our heads clear from all the temporary situations of our lives. The motto of our lives should be *The attitude of gratitude is the secret of a happy life.*

Well, I choose the topic for my thesis. I am very thankful to my guide and friend Dr. Debabrata Deb for letting me work on this topic, in limited stipulated time of my course duration. He has shown full confidence in my instincts and provided all the tools to let me learn and shape things at my own pace. He introduced me to the online course of Computational Material Science by Dr. Stefaan Cottenier, which helped me to learn fundamentals of Density Functional Theory. He supported me not only with his academic knowledge but he also loved to share his personal experiences on the similar difficult situations I was facing. This quality keeps the moral of students high. His acknowledging and appreciative gaze, everlasting smile and poetic style of speech makes him a very vibrant personality as a teacher. Working with Dr. Deb is a lifetime memorable happy experience.

I am very much thankful to my friends, my peer groups, classmates in M. Tech and other scholars in Dr. Deb's lab. They helped me to keep my head clear, remain grounded and devoted to my objectives and yes, leaving me alone whenever I desired and needed to be. For them, a few words of acknowledgment or a simple thanks is not just enough.

I will never be able to count the sacrifices of my parents and will never be able to reciprocate their love in the same way. They supported me in every way to keep my good mental state.

I am little shy to admit that I am a bit jealous of the abilities of my little sis Riya, who is a genius and a literati. Anyway, yes, I like to exploit her abilities.

Above all, I like to thank Lord Kṛṣṇa.

> īśvaraḥ paramaḥ kṛṣṇaḥ
> sac-cid-ānanda-vigrahaḥ
> anādir ādir govindaḥ
> sarva-karaṇa-kāraṇam

I pay obeisances to Lord Kṛṣṇa who is known as Govinda is the Supreme Godhead, who has an eternal blissful spiritual body, is the origin of all, has no other origin and is the prime cause of all causes.

Navdeep

Abstract

Nanoporous materials are of immense scientific and technological interest. The pores present in a material result in the large internal surface area. The nanosized pores, due to the effect of quantum confinement, have certain active sites on the internal surface. By influencing the different microstructure parameters, the properties of nanoporous materials can be tailor-made to suit numerous applications.

The present work is a step towards the development of a generalized algorithm for the modeling of random nanoporous crystalline materials. The methodology is based on the symmetry information of the bulk crystal and the surface energy of the possible cleavage planes. Two generalized methods are proposed for identification of the possible cleavage planes, and the surface energy along these planes is calculated using the DFT energy calculations based on the slab model approach.

The novelty of this work lies in the application of minimum spanning tree algorithms for the creation of the porous network. Distribution of the pore network is affected by the aforesaid parameters. The environment dependent parameters, such as temperature and time of exposure of the sample to the environment, are not yet included in the study and once that is done, the results of the proposed algorithm can be directly compared with the experimental data.

Contents

List of Figures

List of Tables

Chapter 1

Introduction

From the time immemorial, Nature continues to mesmerize humans. Humans are still awestruck by the immense beauty, power and the intricate designs of the Nature. Nature continues to inspire and nurture the development of every aspect of the lives of humans. Designers, scientists and engineers continue to study the complex natural phenomena to create more efficient products or processes [1]. Unveiling the mysteries of the infinite Nature is like walking an infinite staircase. With each new step, there is potential for greater advances in science and technology. However, the progress should be more sustainable with smaller ecological footprint [1, 2]. Scientific enquiry is supported by the three pillars. These three important concepts are experiment, theory and simulation [3]. These are defined with the help of an example of the field of electromagnetism [4]. This field of physics was developed in the 18th century and can be said to be in its infancy stage. In the infancy stage, for any field of science, two things that matter are experiment and theory. One needs to collect a lot of facts, like in this case: observations about electrical phenomena, interactions between charges, the concept of current, etc. One observes nature and conducts experiments. Simultaneously, mathematical foundation is developed that connects these observations with each other. In the beginning, it does not fit well as the new observations may contradict the theory, and so there is a dialogue for a while; but gradually the right theory is developed and so was in the case of electromagnetism illustrated by the instance when Maxwell's equations [4] were finalized. After the development of some robust theory, the field of physics enters its teenage stage. The theory is almost finished and what matters is experiment and simulation. One tries to duplicate experiments by equations. The theory is tested for more and more difficult and complex situations by correlating with experimental data, and if there is no major flaw in the theory, the field of physics becomes mature and the only activity left is simulation. The classical electromagnetism has become mature as nowadays no more experiments are conducted. The field is in the hands of engineers and they build new devices by using Maxwell's equations. There is no experimental phase and that is the signature of a mature field.

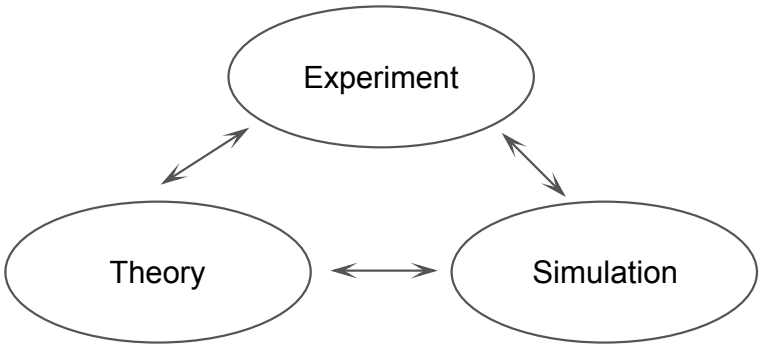

Figure 1.1: Relationship between Experiment, Theory and Simulation

The general intention of scientific enquiry is to gain some knowledge about the natural phenomenon. However, any natural phenomenon is neither too simple nor too obvious that it could be controlled or grasped without abstraction. Scientific abstraction means replacing any natural phenomenon or the real world scenario under study by a model. A model is a simplified imitation preserving all the requisite features of the natural phenomenon. Abstract models can be the starting point of any theory. The principle of modelling or the process of designing models is very useful to understand the field of material sciences, where one works with a large scale variation and mechanisms. Different models in the literature for computational material science can be classified based on different aspects as shown in Table 1.1.

Table 1.1: Categories of Models [5]

Classification aspect	Type of model
spatial scale	macroscopic, mesoscopic, microscopic, nanoscopic
spatial dimension	one-, two-, three-dimensional
spatial discretization	continuum, atomistic
predictive character	deterministic, stochastic/ probabilistic, statistical
descriptive character	first-principles, phenomenological, empirical
path-dependence	kinetic, static

The properties of the engineering materials, like mechanical and electromagnetic properties, not only depend upon the average chemical composition but are also largely influenced by the microstructure. The evolution direction of the microstructure is concluded by thermodynamics and the kinetics selects the evolution path [6]. The microstructure of the engineering materials typically encountered is in the state of non-equilibrium. This non-equilibrium state is looked upon with interest by engineers and scientists, as it invokes large varieties and complexities in microstructure, resulting in advantageous material property profiles. Microstructure can be defined as the amalgamation of all the thermodynamic non-equilibrium lattice defects that range from Angstroms to several meters. Its temporal evolution ranges from picoseconds to years. One of the goals of material sciences is to relate the macroscopic behaviour of the engineering material to its microstructure. Therefore, the study and identi-

fication of different defects and their static and dynamic behaviour on the various properties of the material are of utmost importance. The behaviour of the materials depends upon the thermodynamics and kinetics [6]. Thermodynamics concludes the evolution direction of the microstructure in accordance with temperature, pressure, and so forth; kinetics, depending upon the involved lattice defects that decide microstructure evolution, selects one out of the many possible evolution paths. Therefore, microstructure simulation effort is targeted towards kinetics of microstructure. The details of the simulation include scale and lattice defects. Due to the non-linear character of the microstructure evolution, it is a critical task to decide what details are to be included in the simulation. The aim of the simulations is three-fold [7]. First, to develop better insight of the physical principles that control the microstructure evolution; second, to develop microstructure property relations; and third, to implement both the previous points for the conditions that are not accessible for experimentation or for predicting the results before experimentation. To meet these aims, it is important to identify the proper scales and defects for the simulation. The large spread of scales leads to the introduction of the concept of integration of simulations [7]. This concept helps to bridge the gap amongst different levels of simulation by coupling the codes for different scales. This concept also aims to identify the characteristic scales of microstructure evolution. It identifies upper and lower bounds that limit the application of simulation methods [8]. This decides the scale of simulation whether nanoscale, microscale, mesoscale or macroscale and whether the defects are to be treated individually, collectively or in averaging continuum approach.

The present work deals with nanoscience. In the last few decades, advancement in experimental techniques has led to the development of abilities to manipulate and construct objects at the nanoscale. The branch of nanoscience, for sure, appeared due to the advancement in experimental techniques. Some of the used experimental techniques are as follows [9]:- scanning tunneling microscopy (STM) is the first invention developed to characterize nanoclusters [10]; atomic force microscope, an offspring of STM, not only characterizes the objects at nanoscale but also helps to manipulate them [10]. A variety of other advanced techniques is used to control fabrication of nanotubes and nanocrystals. Fabrication of quantum dots and wells that are entirely a new set of elementary nanoscale particles. Synthesis of biomolecular materials using the genetic techniques and combinatorial chemistry have opened the new arena of research. Development of nanointerfaces and interconnects between hard and soft matter is also widely researched areas.

During the same period, the fundamental techniques used for the modeling and simulation relevant to work at the nanoscale, have also undergone a revolution. The supercomputing performance of the hardware has improved by several orders of magnitude [11] as can be seen from Fig 1.

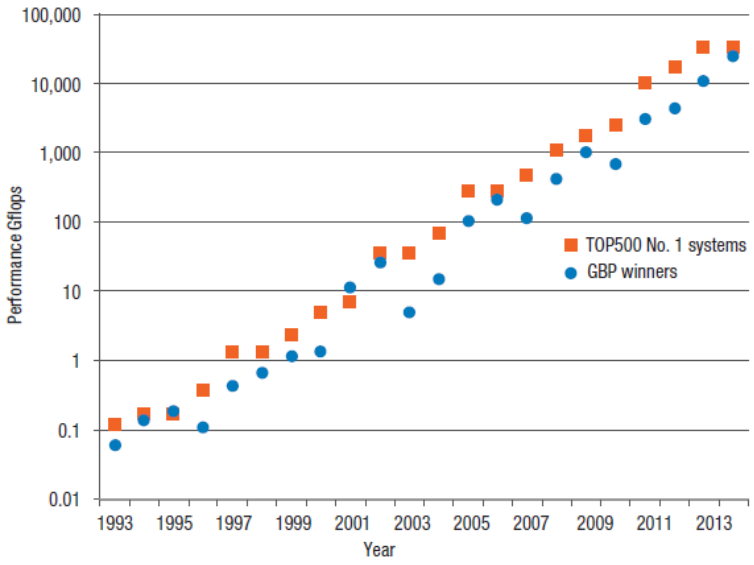

Figure 1.2: Performance of the Gordon Bell Prize (GBP) winners and the TOP500 since 1993 [11].

Other than the continuous improvement in supercomputing performance, the modeling and simulation tools had also undergone much furtherance. For example,

- Density Functional Theory (DFT) [12] helps in predicting "zero Kelvin" properties as it does not account for thermal motions and entropy. This method is about solving the second order Schrodinger wave equation for structures with hundreds and thousands of atoms. This technique had led to the discovery of new materials. More details about DFT including its theory and applications are included in Chapter 3.
- Molecular dynamics [13,14] help in studying the dynamics of a system composed of millions and billions of atoms [15]. This requires the exact solution of many body Schrodinger wave equation. However, the quasi-classical treatment of the atomic interactions and resulting dynamics using classical force fields, is consistent within certain limits, with the solution of Schrodinger equation. There are number of force fields that have been developed to treat all atoms in the periodic table [16], biomolecules [17], and condensed matter [85]. This is a deterministic simulation technique that provides insight into the path dependence of the microstructure evolution at the atomistic level.
- Monte Carlo techniques [13, 19] consist of direct approaches to mimic stochastic events, which can be decomposed into isolated processes and statistical approaches, to integrate multidimensional definite integrals numerically. MC techniques are grouped according to the sampling technique used. They help in the prediction of equilibrium configurations of the system. These techniques are not just confined to nanoscale but to any scale if these are applied to a proper probabilistic model.
- Mesoscale techniques [20] are used to study material properties much beyond atomistic

scale, in which constitutive relations replace the solutions of the equations of motion of all atoms. Some of the typical simulation methods are space-discretized dislocation dynamics, kinetic phase field or generalized Ginzberg-Landau models, deterministic and stochastic cellular automata, kinetic multistate Potts models, geometrical topological and component models, topological network and vertex models.

- Quantum Monte Carlo methods [21] are used to study complex problems related to properties of surfaces and defects, by including electron correlation effects with high precision. These methods are taken as standards against which other techniques may be compared. They provide better results as compared to less demanding density-functional approach and a deeper insight of real materials in terms of electron correlation. High-performance parallel computing is used to run the algorithms for systems containing thousands of electrons.

- Ab-initio Molecular Dynamics methods [22] are used not only to predict "zero Kelvin" properties but also take into account finite temperature motion of condensed matter systems at the atomistic level. The motion of the nuclei follows Newton's equations and is integrated numerically with the finite time step. At each time step, wave function is optimized in the DFT framework. This combines the accuracy of DFT methods and improves the ability to study time dependent phenomena. However, AIMD method is much more computationally demanding than static calculations. These methods are not only limited to study of crystals but applicable to interfaces and complex liquids [23]. AIMD helps in calculating pair distribution functions and coordination numbers that help in predicting the stability of computational materials.

In the last few decades, both the simulation tools and the experimental techniques in relevance to nanoscience have undergone much improvement. This improvement is the true revolution full of numerous opportunities.

High-throughput Density Functional theory is becoming a popular tool for accelerating the development and design of new materials by collecting millions of DFT calculations in large databases. The properties of the new material are predicted by comparing its structure with the materials with the similar structure in the database, as depicted in Fig. 1.3. Data-mining techniques [24] and machine learning models [25] are critical for solving material problems. Experimental synthesis and predictive modeling (such as the GW approximation, the random phase approximation, and quantum Monte Carlo) work simultaneously thus accelerating the development of new materials. Several projects such as Materials Genome Project [26], Open Quantum Materials Database [27], the Computational Materials Repository [28] and AFLOWlib [29] are working and contributing towards new material discovery in the areas of battery materials [30], piezoelectrics [31], nanomedicine [32], perovskites [33] and much more.

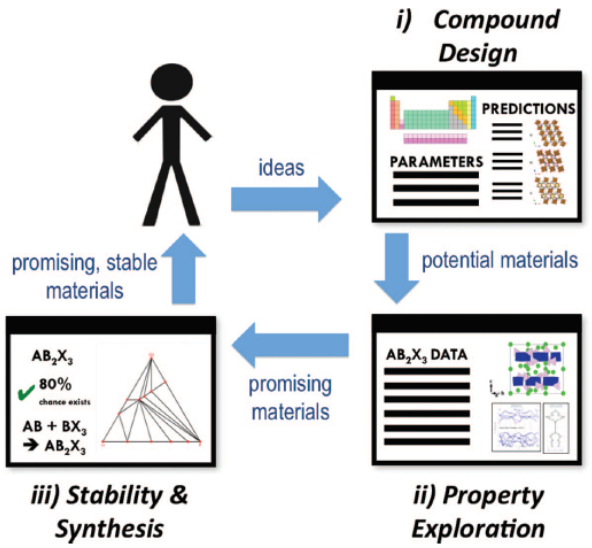

Figure 1.3: Rapid prototyping and iterative materials design steps that might be performed *in silico* [26].

Nanoscience is itself a challenging field that involves multiple spatial and temporal scales and the type of molecules and nanoclusters that are traditionally studied under separate subdisciplines. Some of the challenges or the opportunities in this field [9], from the last decade, that still continue to interest the researchers, are listed below.

- To devise recipies for bridging a wide range of spatial and temporal scales. This will help to model the phenomena captured in the atomistic simulations at the nanoscale and beyond.
- To develop keen insight of transport mechanisms, including electron transport (related to nanowires, nanotubes and molecular electronics), spin transport (related to spintronics-based devices) and molecule transport (related to nanofluids, molecular separations/ membranes and chemical and biological sensors).
- To simulate the optical properties of the nanostructures and to model nanoscale optoelectronic devices with reasonable accuracy .
- To develop theoretical and simulation approaches to quantum coherence and decoherence, including tunneling phenomena, all of which are central issues for using nanotechnology to implement quantum computing.
- To develop theoretical and simulation approaches to study nano-interfaces which are highly complex, heterogeneous and are often related to dissimilar classes of materials.
- To develop theoretical and simulation approaches to spintronics, related to the phenomena in semiconductor based spin valves and spin qubits.
- To simulate complex nanostructures involving several molecular and atomic species and

also to explore combinations of soft organic and hard inorganic structures.

- To develop self-validating and benchmarking methodologies for modeling and simulation at different scales, esp. at nanoscale.
- To develop theoretical and simulation approaches to nano-interfaces between hard and soft matter (related to biomolecular materials and their applications).

Nanoscience is a young exciting interdisciplinary field. Every new finding, whether in terms of some new theory, or improved supercomputing capability, or any innovation in the experimental techniques, the new opportunities and new challenges await. Therefore, this multifarious arena continues to enjoy the limelight and attract the researchers of different fields.

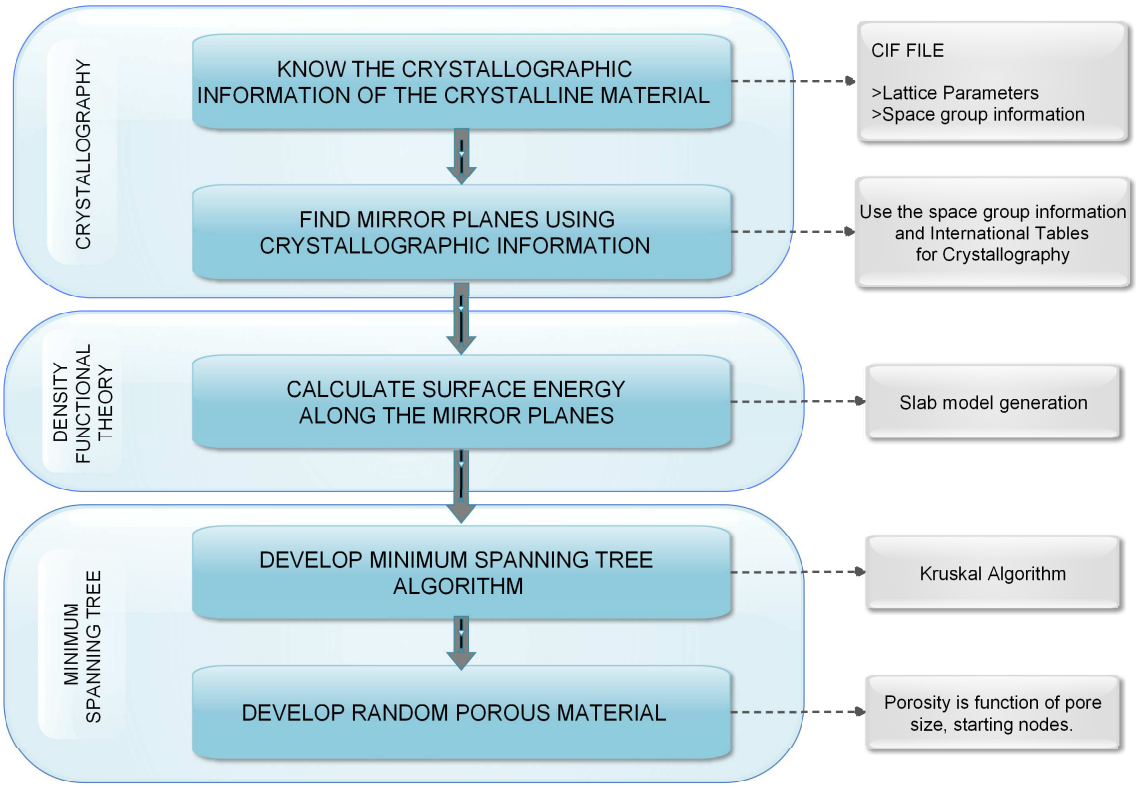

Figure 1.4: Steps for the Proposed Algorithm for the Modeling of Random Nanoporous Material.

The present work concerns with the study of nanoporous materials. Nanoporous materials is a hot field of research due to numerous opportunities [34]. The physics of these nanostructured materials with negative curvature are hard to understand. Many physical quantities, like surface energy, cohesive energy, mechanical modulus, are not constant due to atoms that are under coordinated in the surface layer of low dimensional systems. The inner surface atomic state of nanoporous structures is different from that of multi layers, nanocrystals and bulk counterparts. Thus, the surface energy of the inner surface of nanoporous materials is the most important quantity which is responsible for novel applications [35, 36]. These

materials are used as heterogeneous catalysts [37], adsorbants [38], gas storage [39], filters and sieving membrane [38], drug delivery applications [40], photovoltaic applications [41], photoluminescence applications, low mass high insulation materials, low dielectric constant and supercapacitor applications [42] and more [43].

The present work is a small step towards the development of a generalized algorithm for the modeling of random nanoporous crystalline materials. The methodology is based on the symmetry information of the bulk crystal and the surface energy of the possible cleavage planes. The novelty of this work lies in the application of minimum spanning tree algorithms for the creation of the porous network. Fig.4.4 presents the steps for the proposed algorithm.

Every step of the proposed algorithm is discussed in detail in the forthcoming chapters. Even though the algorithm presented is generalized, the methodology and the results are discussed with the example of nanoporous silicon. Nanoporous silicon is a popular material with several applications in the field of medicine [44], photoelectronic [45] and photovoltaic [45] devices. The proposed methodology is developed based on the experimental and simulation data and other theoretical results. The assumptions, limitations and possible improvements for each step of the algorithm are presented in the concerning section. Instead of moving on to chapter 2, it is advised to start with section 4.2 to quickly grasp the key concepts of the work, modeling requirements, novelties in the work and the need of methodologies mentioned in Chapter 2 and 3.

Chapter 2

Crystallography

The engineering materials can be classified as crystalline and amorphous. The materials encountered in crystalline form have an exceptionally variable appearance which can be understood by single fundamental principle. The nature of the crystalline materials can be grasped by thinking upon the following properties [46]:

- Many crystals, under ideal growth conditions, not only have smooth faces but also have regular geometric shapes.
- The phenomenon of splitting of crystals and resulting into similar smooth surfaces and similar shapes as that of the original crystals is called cleavage. Example: NaCl crystal.
- Pleochroism is the phenomenon of viewing different colors along the different directions of the crystals. This happens due to the difference in optical absorption of light along different directions. Example: Cordierite crystal.
- The surface of some crystals can be scratched by a sharp needle along one direction but not another. Thus, the hardness of the crystal is varied along different directions. Example: kyanite.
- If a thin layer of wax is applied on the face of gypsum crystal and if some heated metal tip is applied to the face, the front of the wax that melts would be ellipsoidal, not circular. This shows that thermal conductivity is more in one direction than the other.

Such behavior, different values of physical quantity along different directions, is called anisotropy. If the values of the physical quantity are equivalent along different directions, then the behavior is said to be isotropic. Crystalline materials are mostly anisotropic in nature. Unlike gases and liquids, crystals have negligible kinetic energy and have high attraction forces between atoms/molecules. This makes the distribution of atoms periodically homogenous and the atomic interactions regularly ordered. Another category of materials, called amorphous, is very viscous as the atoms fail to arrange periodically with the lowering of temperature. Unlike crystalline materials, amorphous materials do not attain lowest

possible energy state. A crystal is defined as an anisotropic homogeneous body with the three-dimensional periodic ordering of atoms, ions or molecules.

The property of anisotropy, responsible for variations of other structure-dependant physical properties along different directions of the crystalline materials, is explored by the first two steps of the proposed algorithm. The discussion of the steps is presented in the following sections.

2.1 Crystallography Information Resources and Tools

The progress of the science depends crucially on the ability to share information and data, in the form of theory and results of experiments and simulations. With the advent of computers and internet, the communication among the researchers has improved remarkably. There must be a common language for the effective communication. A common format for crystallographic information is not only important for sharing experimental results, but also acts as input for much crystallographic software. The crystal structure information is specified using an international file format called crystallographic information file format (or abbreviated as CIF format) adopted by International Union of Crystallography (IUCr) [47]. Crystals studied previously are archived in crystallographic databases. The databases have several hundred thousand of CIF files, that are available for research purpose [48]. Some database for crystalline materials are free, like Crystallographic Open Database (COD) [49], and some are commercial, like International Crystal Structure Database (ICSD) [50]. Materials Project (MP) [51] provides optimized unit cell CIF file.

2.1.1 Downloading the CIF files

CIF files for any known crystalline material can be searched directly on the website of crystallography database [48]. The procedure to download CIF file is shown below.

1. Go to the database website, say COD website [49]. The main page is shown in Fig. 2.1

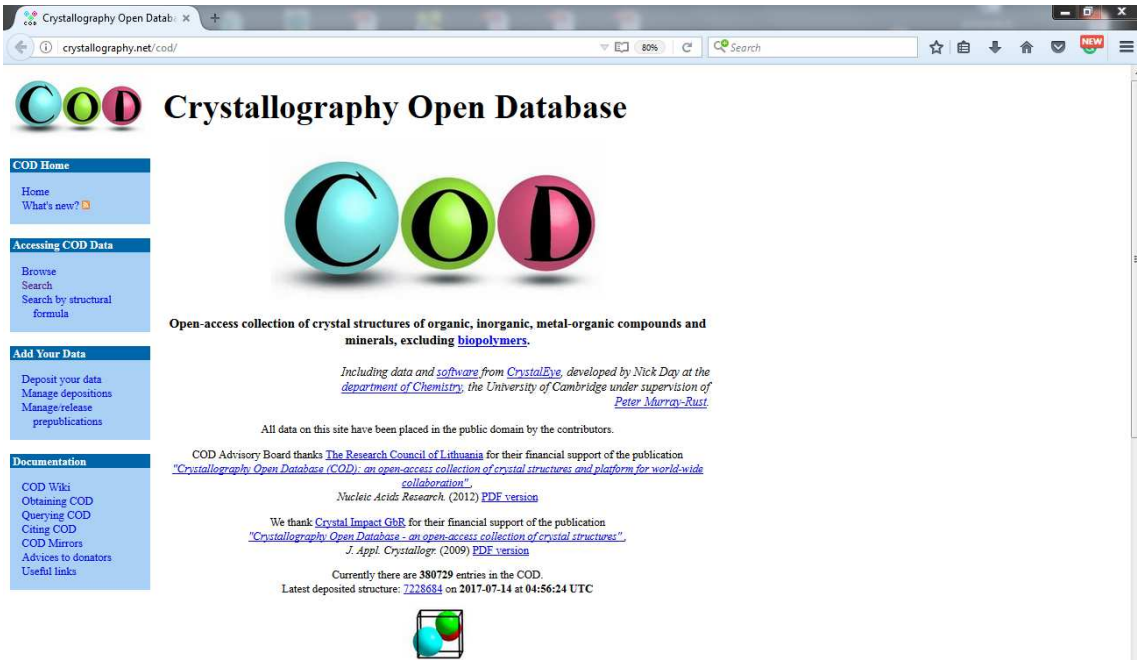

Figure 2.1: Main page of COD website [49]

2. Check category Accessing COD Data and click on Search. The next page shown in Fig. 2.2 display several blanks that ask for the interest of users. Assume, the user needs information on some mineral. Check the online resource to know mineral by its name [52], if required. Suppose the mineral of interest is halite (or NaCl). Enter the Elements and Minimum and Maximum number of elements blanks. Then click on Send.

3. The next screen presents the Search Results shown in Fig. 2.3. Search Results display different entries in the selection. From the presented list, download the desired CIF file. The page also has some crystallographic information of the crystal and necessary references.

CIF file can also be imported using Virtual NanoLab (VNL). Check online reference for the involved steps [53].

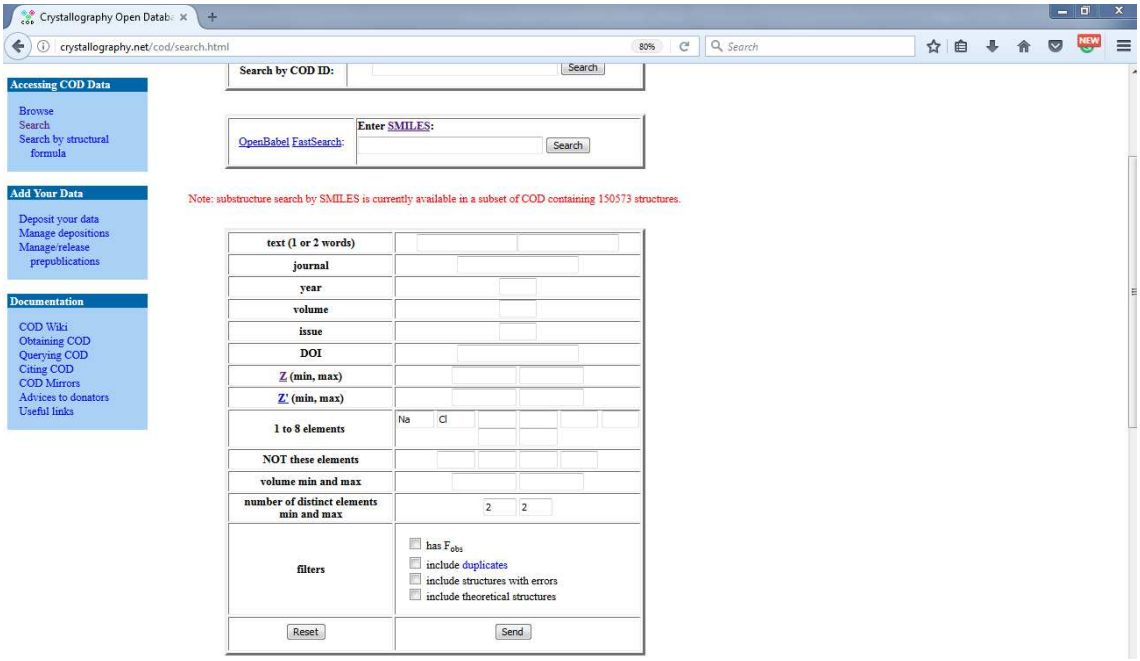

Figure 2.2: Search page of COD website.

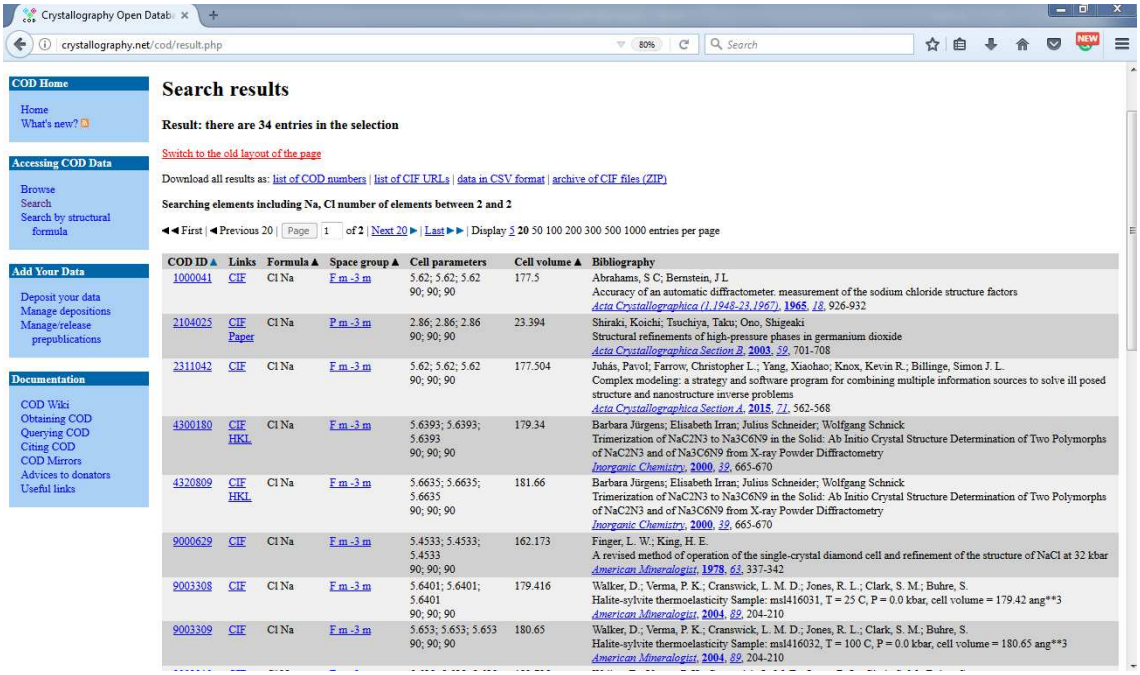

Figure 2.3: Search results for halite crystal on COD database.

CIF file provides a lot of crystallographic information [54]. The minimalistic crystallographic information is as follows.

1. Crystal data loop of the CIF file holds crucial crystallographic information.

   - Lattice parameters: a, b, c are the lengths of unit cell and α, β and γ are the angles of unit cell. The unit of length is angstrom(Å) and of angles is degrees(°).

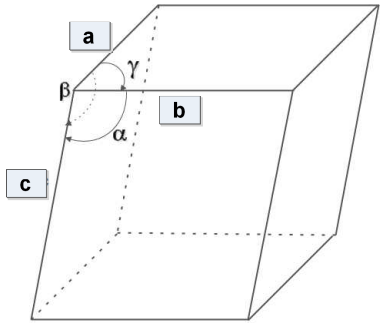

Figure 2.4: Lattice Parameters of the crystal.

   - Symmetry space group (symmetry_space_group_name_H-M): Space group information is given in the H-M notation, i.e., Hermann Mauguin notation [55]. These international symbols indicate the symmetry of the space group very clearly.
   - Number of space group (space_group_IT_number): According to International Tables of Crystallography all the crystals in nature can be specified using 230 space groups [56].

   The information, about lattice parameters, symmetry space group and its number, is presented in the crystal data loop of the CIF file. Part of crystal data loop of the downloaded halite CIF file [57] is shown in Fig 2.6.

```
loop_
_atom_site_label
_atom_site_type_symbol
_atom_site_symmetry_multiplicity
_atom_site_Wyckoff_symbol
_atom_site_fract_x
_atom_site_fract_y
_atom_site_fract_z
_atom_site_thermal_displace_type
_atom_site_occupancy
Na1 Na 4 a 0.0 0.0 0.0 Biso 1.0
Cl1 Cl 4 b 0.5 0.5 0.5 Biso 1.0
```

Figure 2.5: Atomic parameters and displacement parameters loop in the halite CIF file.

```
_journal_issue                   6
_journal_name_full               'Acta Crystallographica Section B'
_journal_page_first              701
_journal_page_last               708
_journal_paper_doi               10.1107/S0108768103021761
_journal_volume                  59
_journal_year                    2003
_chemical_formula_sum            'Cl Na'
_chemical_formula_weight         58.44247
_chemical_name_systematic        ' sodium chloride'
_space_group_IT_number           221
_symmetry_cell_setting           cubic
_symmetry_space_group_name_Hall  '-P 4 2 3'
_symmetry_space_group_name_H-M   'P m -3 m'
_cell_angle_alpha                90.0
_cell_angle_beta                 90.0
_cell_angle_gamma                90.0
_cell_formula_units_Z            1
_cell_length_a                   2.8600(3)
_cell_length_b                   2.8600(3)
_cell_length_c                   2.8600(3)
_cell_volume                     23.394(4)
_cod_data_source_file            ws0004.cif
_cod_data_source_block           II_phase_2
_cod_original_cell_volume        23.393(4)
_cod_database_code               2104025
```

Figure 2.6: Part of crystal data loop in the halite CIF file.

```
loop_
_symmetry_equiv_pos_site_id
_symmetry_equiv_pos_as_xyz
1 x,y,z
2 -x,-y,z
3 -x,y,-z
4 x,-y,-z
5 z,x,y
6 z,-x,-y
7 -z,-x,y
8 -z,x,-y
9 y,z,x
10 -y,z,-x
11 y,-z,-x
12 -y,-z,x
13 y,x,-z
```

Figure 2.7: Starting part of the symmetry loop in the halite CIF file.

2. The symmetry information of the crystal is explicitly written in the symmetry loop of the CIF file. More discussion about this topic is done in the next section. Part of the symmetry loop of the halite file is shown in Fig 2.7 .

3. The keywords in another block shown in Fig. 2.5 refer to atomic coordinates and displacement parameters. The keyword label refers to different atomic species present in the crystal, *symmetry_multiplicity* depicts number of atoms of that species in the unit cell. Wyckoff symbol represents high symmetry position in the unit cell [58]. Three coordinates (x, y and z) specify the position of one of the n atoms. Position of other atoms can be located by knowing the position of one atom and Wyckoff symbol. The possible Wyckoff positions for any space group can be found using Bilbao Crystallographic Server [59].

2.1.2 Visualizing the CIF file

CIF files can be visualized using various tools. These tools also help to retrieve other information, like the distance between atoms and possibly much more, as well.

1. **VESTA** (Visualization for Electronic and STructural Analysis) This is a local crystal

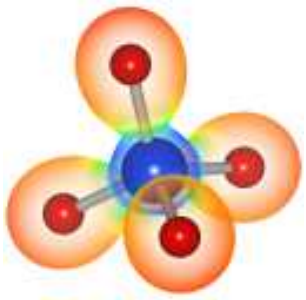

Figure 2.8: VESTA software logo.

viewer that has numerous features [60]. All the crystal structures in this work after this section are presented using VESTA. Crystal structure of halite from the downloaded CIF file [57] is as shown in Fig. 2.9.

2. CIF files can also be visualized online using Bilbao Crystallographic Server [61] if no crystal viewer is present on the system (laptop). The online visual for halite crystal structure is shown in Fig. 2.10.

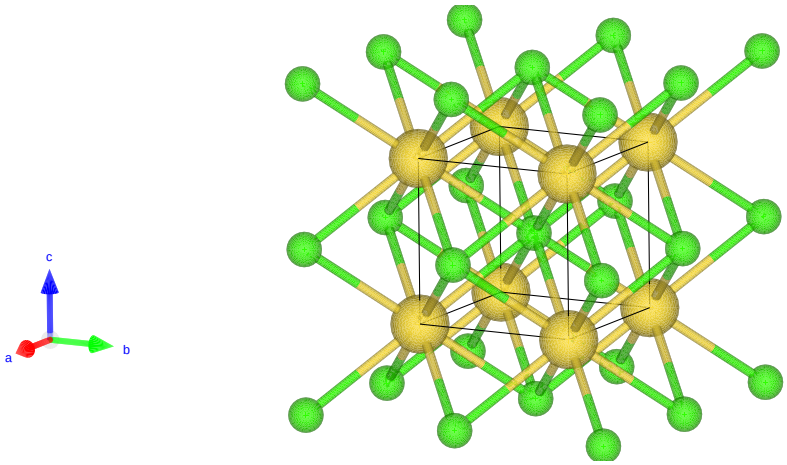

Figure 2.9: Crystal Structure of Halite.

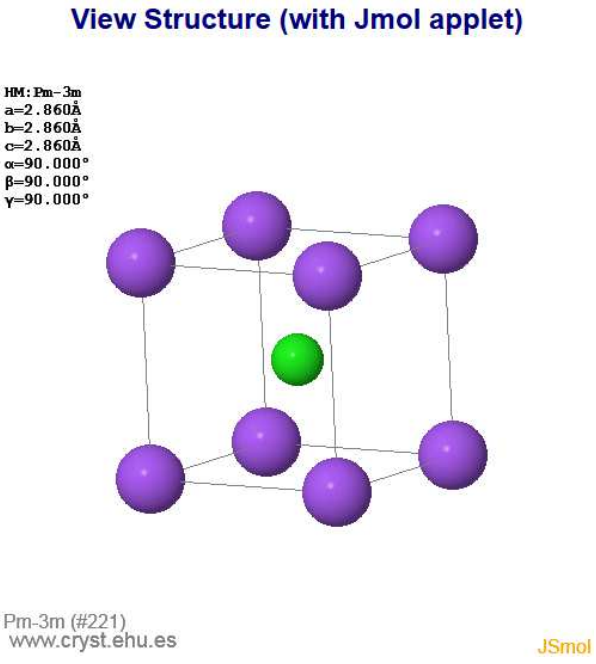

Figure 2.10: Crystal Structure of Halite generated using Bilbao Crystallographic Server.

2.1.3 Creating a CIF file

Following are the steps to create a CIF file:

1. Enter the crystallographic information, without any symmetry information, in the minimalistic CIF file, shown in Fig. 2.11.

```
##########################################################################
######
# general-purpose P1 cif
##########################################################################
######

data
_cell_length_a                      x.xxxxxx
_cell_length_b                      y.yyyyyy
_cell_length_c                      z.zzzzzz
_cell_angle_alpha                   aa.aaaaaa
_cell_angle_beta                    bb.bbbbbb
_cell_angle_gamma                   cc.cccccc
 symmetry space group name H-M      'P 1'
_symmetry_Int_Tables_number         1
loop_
_symmetry_equiv_pos_site_id
_symmetry_equiv_pos_as_xyz
   1   'x, y, z'

loop_
 atom site label
_atom_site_fract_x
_atom_site_fract_y
_atom_site_fract_z
Fe1   0.743210   0.330733   1.032268
#End of data_P1
```

Figure 2.11: Minimalistic CIF file.

2. This CIF file cannot be used directly as it is very basic and may have syntax errors. The necessary information can be retrieved by passing through Bilbao Crystallographic Server [61]. Upload this old CIF file and download new CIF file. This new file still doesn't have symmetry information.

3. Symmetry information for the CIF file can be obtained using FINDSYM online tool [62, 63]. The new CIF file, if devoid of any major errors, can be successfully uploaded to the server. Sometimes the atomic positions in the CIF file are not fully exact, as underlying symmetry may be obscured due to some noise. There is an option available for setting the tolerance for uploaded data.

4. After submitting the data a new CIF file is generated, that contains the symmetry information. This new file can run any DFT code more efficiently than the previous data file.

The other method to create CIF file is by using Virtual NanoLab (VNL) [64].

2.2 Symmetry Information of the Crystal

The objective of this section is to find the planes that are parallel to some special projections. The projection plane is normal to projection direction. This is done to ensure that all the spherical atoms appear circular on the projection plane. The projection directions correspond to the primary, secondary and tertiary symmetry directions of the lattice cell. They are taken along coordinate axes if the lattice lacks symmetry. Projection directions for different crystal systems are listed in the Table 2.1.

Table 2.1: Projection Directions for the Crystal System [65]

Crystal System	Projection Directions
Triclinic	[001] [100] [010]
Monoclinic	[001] [100] [010]
Orthorhombic	[001] [100] [010]
Tetragonal	[001] [100] [110]
Hexagonal	[001] [100] [210]
Rhombohedral	[111] [$1\bar{1}0$] [$2\bar{1}\bar{1}$]
Cubic	[001] [111] [110]

The focus is to calculate surface energy for the planes parallel to any projection direction using the Density Functional Theory simulations. The choice of special projections is quite reasonable, pertaining to the symmetry of the crystal, as this limits the simulation load and thus seems to be a good assumption. Due to the anisotropy, the surface energy along different directions is believed to be different, this topic is dealt in next section.
In this section, the required planes are found using the information from the CIF file, i.e., lattice parameters and space group. Consider the example of Silicon. The CIF file is downloaded from COD database [66] following the steps mentioned in the previous section. The unit cell of the silicon is shown in Fig. 2.12. A part of Crystal data loop of Si is shown in

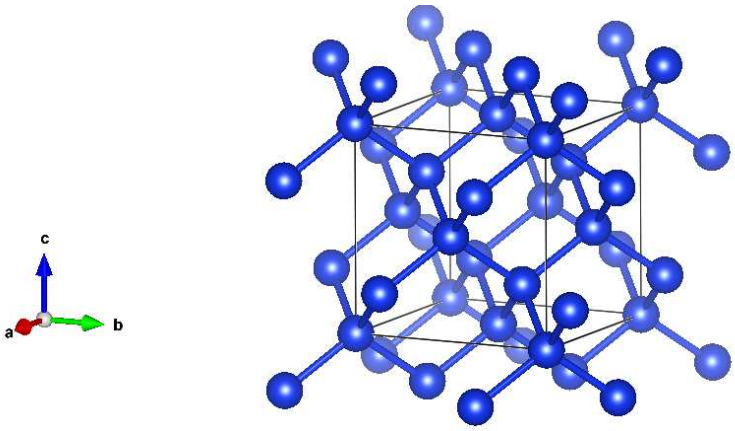

Figure 2.12: Silicon unit cell.

Fig. 2.13. The necessary information taken from the CIF file is shown in Table 2.2.

```
_chemical_formula_sum              Si
_chemical_name_common              Silicon
_space_group_IT_number             227
_symmetry_space_group_name_Hall    'F 4d 2 3 -1d'
_symmetry_space_group_name_H-M     'F d -3 m :1'
_cell_angle_alpha                  90
_cell_angle_beta                   90
_cell_angle_gamma                  90
_cell_length_a                     5.43070
_cell_length_b                     5.43070
_cell_length_c                     5.43070
_cell_volume                       160.165
_diffrn_ambient_temperature        1573
_exptl_crystal_density_diffrn      2.329
_cod_original_sg_symbol_H-M        'F d 3 m'
_cod_database_code                 9008566
```

Figure 2.13: Minimalistic CIF file.

Table 2.2: Lattice parameter and Symmetry information from Silicon CIF file

Parameter	Value
a	5.4307 Å
b	5.4307 Å
c	5.4307 Å
α	90°
β	90°
γ	90°
Space group(in H-M notation)	Fd$\bar{3}$m
# of space group	227

It is easier to work with two-dimensional projections as compared to working with three-dimensional crystals. In this section, two methods are proposed to find the planes that are normal to special projections. The first method is developed using concepts in International Tables of Crystallography-Vol A (ITA) based on the space group information of the unit cell. The second method is developed using stereographic projections based on the lattice parameter information.

2.2.1 Method 1

The steps of the proposed algorithm are as follows.

1. Collect the space group information from the CIF file.
2. Follow the corresponding space group chart from ITA and note the block 'Symmetry of Special Projections'.
3. From the block, note the projection directions for the unit cell and corresponding plane

groups along these directions.

4. Look at the corresponding plane group chart from ITA and note the block 'Symmetry Operations'.
5. In this block, note the mirror symmetry lines and the coordinate.
6. This information corresponds to the required planes.

The steps of the proposed algorithm are explained with the help of example of Silicon. As reported in Table 2.2, space group number for Silicon is 227 and space group is $Fd\bar{3}m$ with the origin choice 1. Space group information chart is presented in the Appendix.

The plane groups along special projection directions can be deduced from the Symmetry of Special projections block. The deduced information is shown in Table 2.3. The plane group

Table 2.3: Plane group symmetry along special projection directions for Si unit cell.

Special Projection Directions	Plane groups
[001]	p4mm
[111]	p6mm
[110]	c2mm

information chart for these plane groups is presented in the Appendix. The information that helps in deducing the planes normal to projection direction is shown in Table 2.4.

Table 2.4: Symmetry information of plane groups

Plane groups	Symmetry operations	Symmetry elements
p4mm	(1) 1 (2) 2 0,0 (3) 4^+ 0,0 (4) 4^- 0,0 (5) m 0,y (6) m x,0 (7) m x,x (8) m x,$\bar{x}$	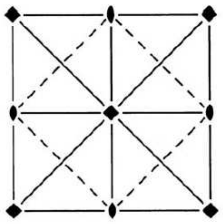
p6mm	(1) 1 (2) 3^+ 0,0 (3) 3^- 0,0 (4) 2 0,0 (5) 6^- 0,0 (6) 6^+ 0,0 (7) m x,$\bar{x}$ (8) m x,2x (9) m 2x,x (10) m x,x (11) m x,0 (12) m 0,y	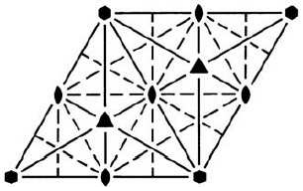
c2mm	For (0,0)+ set (1) 1 (2) 2 0,0 (3) m 0,y (4) m x,0 For $(\frac{1}{2},\frac{1}{2})$+ set (1) $t(\frac{1}{2},\frac{1}{2})$ (2) 2 $\frac{1}{4},\frac{1}{4}$ (3) b $\frac{1}{4}$,y (4) a x,$\frac{1}{4}$	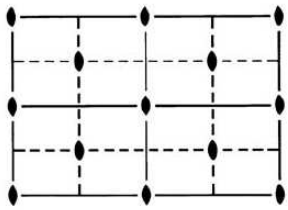

The steps of the proposed algorithm are like looking at the unit cell from different special projection directions, as shown in Fig. 2.14. These directions are marked as special as the symmetry of the plane projections can be categorized by one of the 32 plane groups.

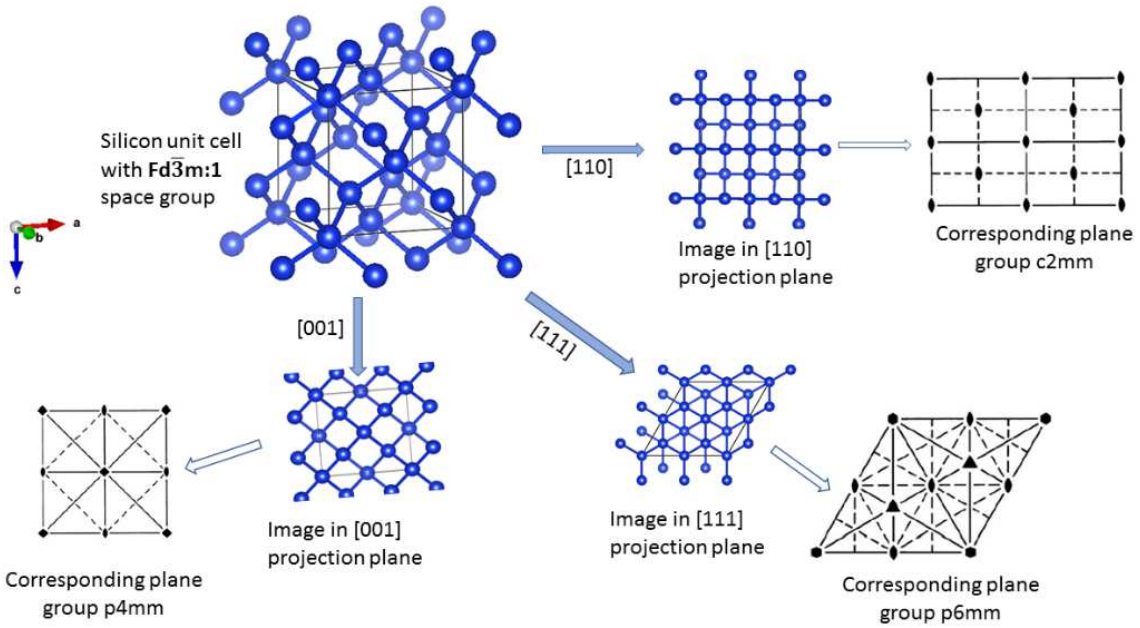

Figure 2.14: The steps for the proposed algorithm of Method 1, illustrated with the help of Silicon unit cell.

There are different symmetry operations; rotation, reflection, inversion, and lattice translation. They may be linked together to form compound symmetry operations as shown in Table 2.5 below. The corresponding symmetry elements are in round brackets.

Table 2.5: Symmetry information of plane groups [71].

	Rotation	Reflection	Inversion	Translation
Rotation	x	Roto-reflection	Roto-inversion	Screw Rotation
Reflection	(Roto-reflection axis)	x	2-fold rotation	Glide reflection
Inversion	(Roto-inversion axis)	(2-fold rotation axis)	x	Inversion
Translation	(Screw axis)	(Glide Plane)	(Inversion centre)	x

A symmetry element in the space group does not project as the symmetry element unless it bears a special relation with the projection direction. All the translation components of the symmetry elements along the projection direction disappear, while that are perpendicular to projection direction may be retained [72].

Cleavage of the crystal along the reflection planes yields the symmetrical faces. The mirror

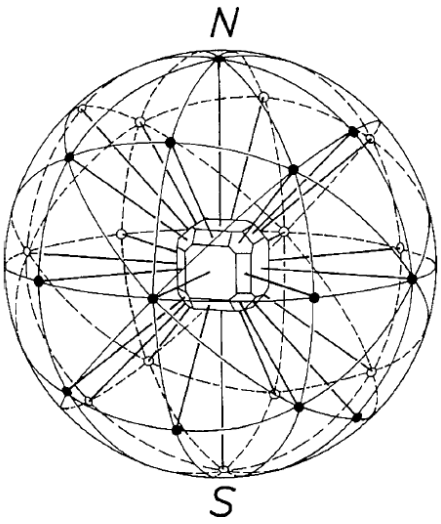

Figure 2.15: Normal to the faces of the crystal cut the sphere at poles. The poles lie on the great circles [73].

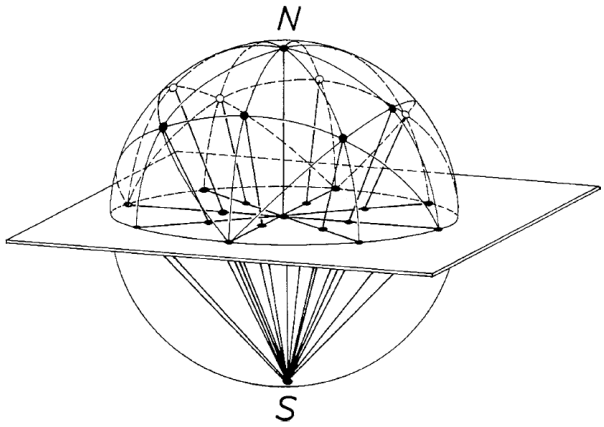

Figure 2.16: Stereographic Projection [73].

lines in the projections usually correspond to the reflection planes parallel to the projection direction [72]. Otherwise these may correspond to the glide planes that do not have any component parallel to projection plane [72]; or mirror lines may be due to the n-fold rotation or n-fold screw axis (with n even) normal to projection direction [72]. These may correspond to possible anomalies in more complex symmetries. Development of robust mathematical techniques for eliminating these anomalies can be a part of the future work.

Considering the mirror lines in plane groups of the special projections, taking care of the possible anomalies in this method, and the high symmetry of the silicon crystal- the chosen family of reflection planes is shown in Table 2.6.

Table 2.6: Family of planes parallel to special projection directions.

Special Projection Directions	Chosen family of planes
$\langle 001 \rangle$	$\{001\}, \{110\}$
$\langle 110 \rangle$	$\{001\}, \{110\}, \{111\}$
$\langle 111 \rangle$	$\{110\}, \{211\}$

The results can be verified from the other proposed method. The mathematical proof of the imagination, for drawing a plane parallel to the given direction through a normal mirror line on projection plane, is the part of future work.

2.2.2 Method 2

The second method is based on the concepts of stereographic projections. Its principle can be shown in Fig. 2.15.

Consider a crystal in the center of the sphere. The normal to each crystal face, starting from the center of the sphere, intersects with the surface of the sphere at certain points called poles of the faces. These poles are not randomly distributed but lie on some great circles, the largest possible circles on the sphere with radius same as the sphere. The crystal faces belong to the same zone if their poles lie on the same great circle. The zone axis will lie normal to the plane of the great circle. Assume the sphere to be a terrestrial globe with Northern and Southern hemisphere as shown in Fig. 2.16. The lines from the poles in the North hemisphere are projected on the South pole. The intersection of these lines with the equatorial plane is marked with a dot. Similarly, the lines from the poles in the Southern hemisphere can be projected on the North pole. The intersection of these lines with the equatorial plane is marked with O. The equatorial plane can be said to be stereogram or a stereographic projection.

As mentioned before in this section, the objective is to find the planes that are parallel to some special projections. This objective can be achieved by considering projection direction parallel to the zonal axis. The great circle normal to the zone axis bears traces of the required planes. The methodology is presented with the help of the example of the silicon crystal.

The stereogram is drawn using the lattice parameter data from the CIF file. For the silicon unit cell, the lattice parameter data is shown in Table 2.2.

Wulff net is a kind of graph used for plotting measured crystal angles and that results in a stereographic projection [74].

The six faces $(100), (\bar{1}00), (010), (0\bar{1}0), (001), (00\bar{1})$ can be easily plotted on stereogram. These faces lie along the zone circles: $[100] \equiv [(010)/(001)], [100] \equiv [(010)/(001)]$ and $[100] \equiv [(010)/(001)]$. Zone axis is normal to the plane of zone circle.

Traces of the plane (101) and (011) belong to the [010] and [001] zone circles respectively. The position of the poles of the planes on the respective zone circle is found easily as shown in Fig 2.17 and Fig. 2.18.

Section parallel to (010) is shown in Fig. 2.17. Traces of the planes $(001), (101)$ and (100) belong to the zone (010). δ is the angle between normals to (001) and (101). Section parallel to (100) is shown in Fig. 2.18. Traces of the planes $(001), (011)$ and (010) belong to the zone (100). δ' is the angle between normals to (001) and (011).

$$\delta = tan^{-1}\left(\frac{|\vec{a}|}{|\vec{b}|}\right)$$

$$\delta' = tan^{-1}\left(\frac{|\vec{c}|}{|\vec{b}|}\right)$$

The angles give the position of the poles of the (110) and (011) plane. The position of the poles of the other planes in $\langle 110 \rangle$ family, due to the symmetry, is known, and the poles can be placed in the stereogram. Great circles can be drawn passing through these poles. Similarly, the position of the poles of the planes in $\langle 110 \rangle$ family can be deduced.

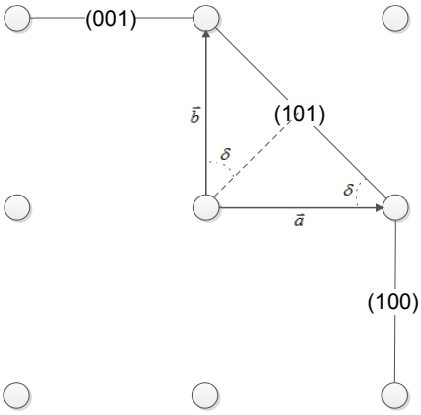

Figure 2.17: Section parallel to (010).

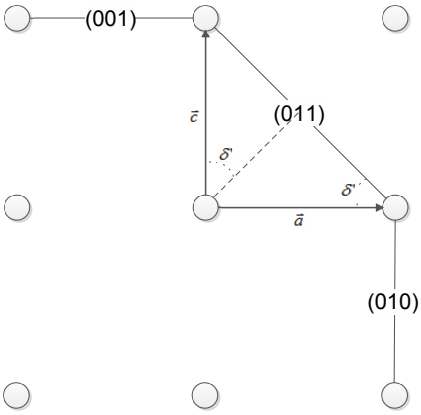

Figure 2.18: Section parallel to (100).

The indexing of the stereogram may seem cumbersome but can be done easily by using complication rule. According to this rule, all the faces of the same zone are indexed by addition or subtraction of the indices of two standard faces.
The crystal at the center of the sphere is tilted, along with special projection directions, [001], [110] and [111], such that projection direction coincides with the N-S axis. The resulting stereograms are shown in Fig 2.19.
The projection direction coincides with the zonal axis. The great circle, normal to the zonal axis, holds traces of some planes. These planes are the required planes parallel to special projection direction. For the Si crystal, the required planes are reported in Table 2.7.

Table 2.7: Family of planes parallel to special projection directions.

Special Projection Directions	Chosen family of planes
$\langle 001 \rangle$	$\{001\}, \{110\}$
$\langle 110 \rangle$	$\{001\}, \{110\}, \{111\}$
$\langle 111 \rangle$	$\{110\}, \{211\}$

The results produced by this method are same as that by first method. This shows both the methods are complementary.

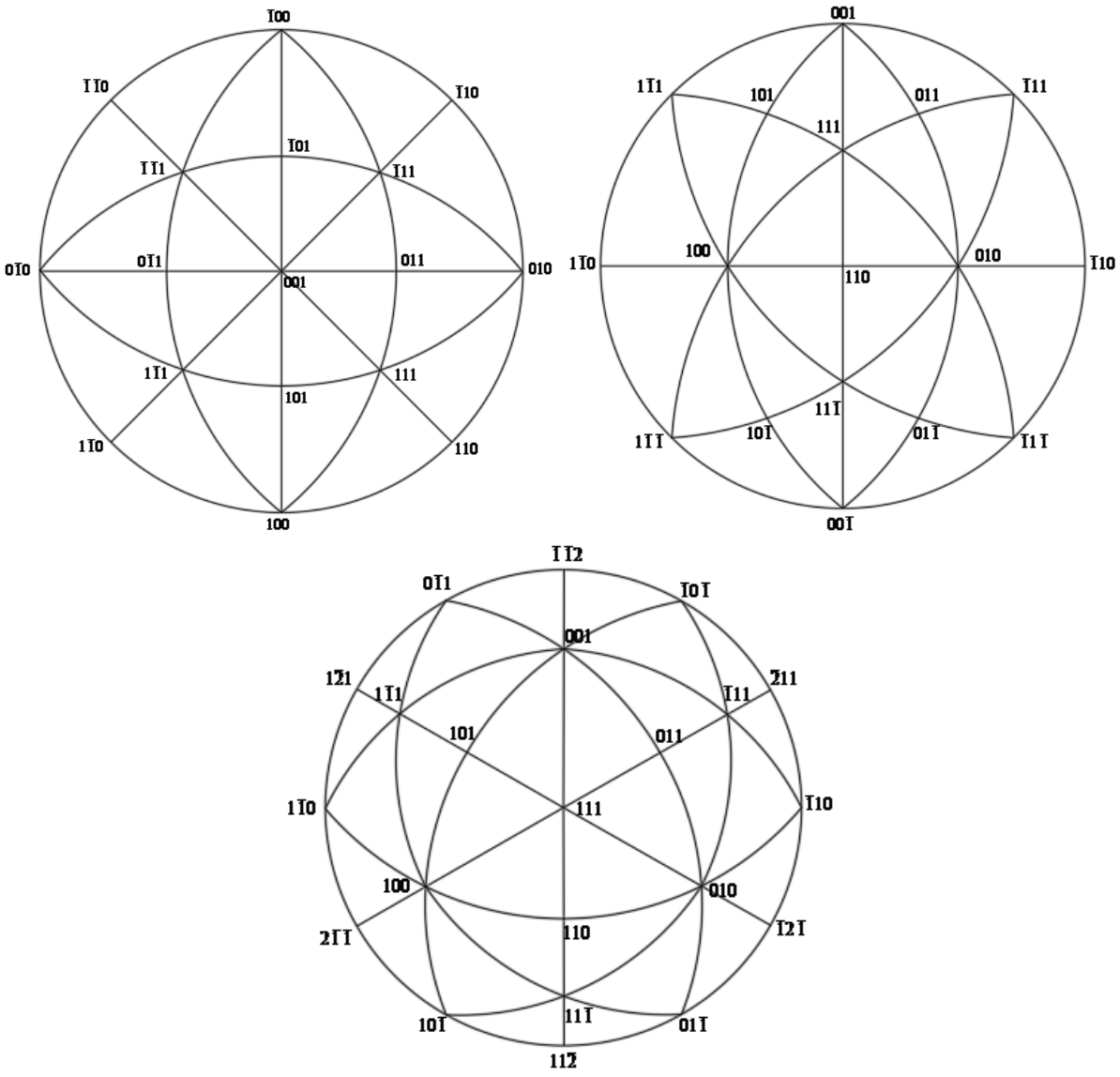

Figure 2.19: The stereographic projections along special projection directions [001], [110] and [111].

Chapter 3

Surface Energy and Density Functional Theory

Apart from having defects, crystals are not infinite either, they are terminated by surfaces. The knowledge of the surface properties of the materials has opened the area of new technologies. For instance, technologies such as solar cells [45] and catalysis [75] involve surface driven processes. Surface properties affect the functioning of nanomaterials, where the relatively large surface area to volume ratio, due to the internal surface area, leads to properties that differ significantly from the bulk materials [76]. Surfaces are created by the expenditure of energy and its value depends upon the type of material and the orientation of the surface. For example, cutting a crystal surface along (100) plane takes different energy from that of (110) plane. Stability of a surface depends upon the surface energy of the material. The measure of excess energy on the surface compared to the bulk is due to several factors, such as broken bonds that lead to under coordinated atoms. Surface energy helps to determine and understand the surface structure, roughening, reconstruction and equilibrium shape of the crystal [77]. Though the surface energy is very important fundamental quantity still it is not very easily measured or determined experimentally, especially along specific facets for most elements [78, 79]. As the material is composed of irregular microcrystals, so the experimental determination of surface energy presents the average value of surface energy along different facets. Table 3.1 shows the distribution of surface energy, calculated experimentally, in the periodic table of elements.

Ab-initio computations or first principle computations, such as those based on Density Functional theory, are important complementary tools to experimental techniques for determining the surface characterization of the properties of the material. First principle calculations cover up the limitations of the experimental techniques, as these help in determining facet specific surface energies [81], morphologies of the nanocrystals, reconstruction of the structures [106], work functions [82], surface electronic structures, adsorbate interactions [83] and much more [84]. The focus of the study is limited only to determining of facet specific surface energies.

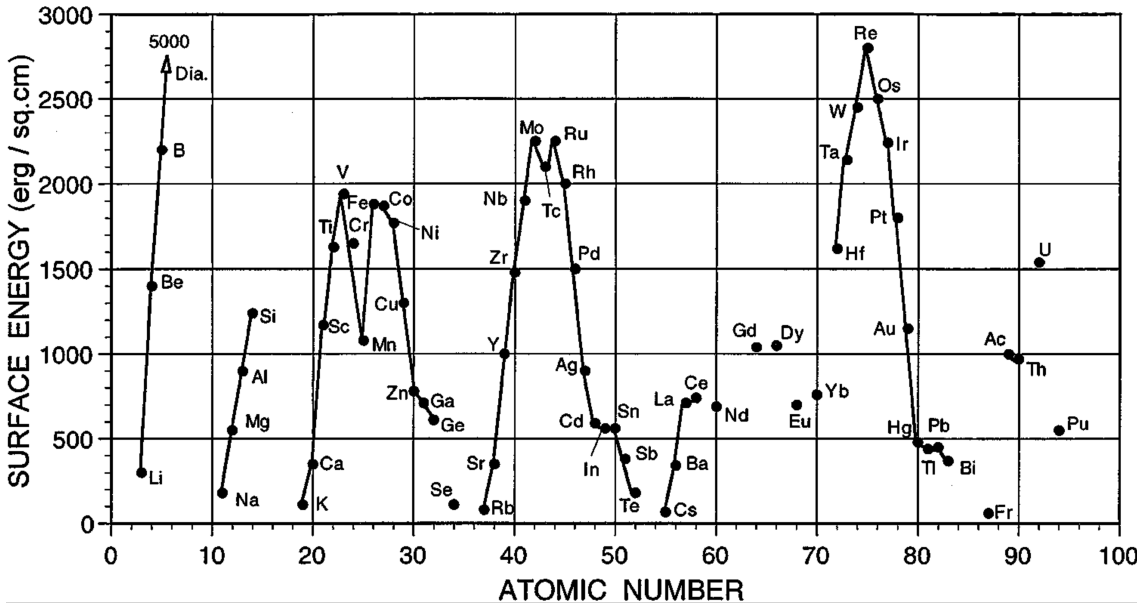

Figure 3.1: The surface energy distribution, calculated experimentally, in the periodic table of elements [80].

3.1 Slab Model Approach

Slab model approach is an ab-initio or first principle method based on the DFT to determine the surface energy of the material along specific relevant facets of interest. Generalised procedure [85, 86] for estimating the surface energy using DFT is presented below.

1. Start from the conventional unit cell (CUC).
2. Preparation of the oriented unit cell (OUC).
   - Prepare the OUC scaling matrix, such that a and b vectors of the OUC are parallel to the plane hkl of required facet of the conventional unit cell. Check the reference [85] for detailed procedure.
   - **c** is chosen to the nearest Bravias point and may not be orthogonal to the plane of **a** and **b**. Check the reference [85, 86] for detailed procedure.
3. The prepared OUC is fully relaxed in terms of its geometry and atomic positions. The total energy per formula unit is determined for the relaxed OUC bulk solid.
4. Create the slab model.
   As a and b lie parallel to the facet under consideration, a supercell is created by extending the multiples of **c** vector. By removing some of the layers of atoms parallel to the required facet, a layer of vacuum is introduced.
5. If the unit cell is large in terms of a number of atoms, it can be reduced by decreasing number of atoms using cell reduction techniques [87]. These techniques assist in

reducing computation time and thus make computations more efficient.

6. If OUC scaling matrix is such that its determinant is equal to 1, then the use of cell reduction techniques can be minimized. Determinant should be greater than 1 and never less than 1, else right handed coordinate system gets transformed to left handed one and vice-versa. If the determinant is equal to zero, then the vectors of the scaling matrix are linearly dependant and do not form a complete coordinate system. [88].

7. By using the same set of input parameters as for calculating the bulk cell, the slab is relaxed in the atomic positions keeping the volume fixed and the energy of slab is determined. If there are a large number of layers, it is advisable to keep atoms of some of the inner layers fixed and then optimize the rest. The effect of vacuum on the atomic positions while moving away from the surface keeps on reducing.

8. The surface energy E_{surf}^{hkl}, required to create the facet with Miller index (hkl) from the bulk is given by the following expression,

$$E_{surf}^{hkl} = \frac{E_{slab}^{hkl} - n_{slab} \times E_{bulk}^{hkl}}{2 \times A_{slab}} \tag{3.1}$$

   Where E_{slab}^{hkl} is the total energy of the slab model, n_{slab} is the number of formulae units in the slab. E_{bulk}^{hkl} is the energy per formula unit of OUC, the factor 2 in the denominator accounts for the two surfaces of the slab model, and A_{slab} is surface area of slab structure.

   The tacit assumption of the $\frac{1}{2}$ factor means that the slab has identical terminations, and both the terminations contribute equally to the surface energy. However, identical terminations are possible only when the center of the slab has appropriate symmetry. If the symmetry operations are not at the center than the calculated energy is instead cleavage energy'. This energy is not same as surface energy and is defined as the reversible work done per unit area required to separate an infinite bulk from the plane. If the $\frac{1}{2}$ factor assumption is not valid due to non-occurrence of symmetry then the duplicate surfaces of the slab are reconstructed [85]. This work is limited only to unreconstructed surface energies. The study of surface energy for the reconstructed surfaces can be part of the future work. The reconstruction of the surfaces is not explored due to the larger supercell requirement.

9. Verify the slab model if it is good for semi-infinite solid. That means verify the stability of surface energy w.r.t. slab thickness and vacuum thickness.

3.2 Accuracy and Precision of DFT calculations

Accuracy and precision are very important terms that describe the use of any scientific data. It is an important topic that needs to be addressed before working out any DFT calculations.

The single calculated energy term for any computation is not a useful information unless it is compared with other series of calculations to deduce some useful information. The accuracy and precision of the information from DFT are controlled by the following factors.

- **Pseudopotentials** Pseudopotentials are made for a particular exchange correlation functional. This is the important concept in achieving the convergence of the Kohn-Sham problem [89, 90]. In terms of physical quantities, like chemical bonding and other characteristics of the materials, these are mainly characterised by outer electrons or valence electrons. Instead of considering all the electrons in any calculation, just outer shell or valence electrons are considered. Calculations become less computationally demanding by freezing the core shell electrons [91]. This central problem is solved by different ways depending upon the choice of numerical method or exchange correlation functional. Each pseudopotential, like norm-conserving [92, 93], ultrasoft pseudopotentials [94], projector-augumented wave (PAW) [**?**] or plane wave [96] give different details. Each method has its own advantage, it is desirable to achieve high precision. Depending upon the ability of pseudopotentials, these are characterised as Jacob's ladder and hybrid potentials [97]. The reproducibility of the DFT calculations is improving with the better pseudopotentials using different DFT codes [98].

- **Reciprocal Space Sampling (k-point sampling)** By the construction of reciprocal space, every observable property of the solid is described as integral over the Kohn-Sham orbitals. These are labeled by a quantum number k and integral goes over the entire volume in real space. In reciprocal space, the entire space of real space is restricted to first Brillouin zone. Therefore, many properties in the DFT code are obtained from an integral over the first Brillouin zone. The integral is solved not analytically but numerically by replacing it with summation over a few sampling points. More are the number of sampling points better the accuracy of the numerical solution towards the exact solution. Therefore, it is mandatory to find out the number of sampling points for any DFT calculation to achieve the desired accuracy.

- **Basis set size** Many DFT calculations are based on the basis set'. The Kohn-Sham orbitals are expressed on the basis of infinite dimensionality. It is like expressing any periodic function in an infinite basis of cosine functions. As the calculations done by a computer are numerical but not analytic, therefore such an infinite basis set must be truncated. This will limit the precision of the calculation. Ideally, the user should truncate the basis set only after the point where adding more basis information does not affect the result anymore.

The proper choice of pseudopotentials is the responsibility of the user, depending upon the type of solid and property studied. The right choice of the pseudopotential leads to the better accuracy of the data. The choice for the number of reciprocal space sampling points

and basis set size should be done after the proper convergence testing. This is the testing technique in which the number of sampling points and basis set size is worked out such that the resultant calculations produce data within the precision range. This information has to be documented properly in research articles to ensure of the numerical stability of the provided results.

3.3 Calculations

As mentioned in Chapter 1, all the methodologies and recipes for the various steps for the development of the generalized proposed algorithm for the modeling of random nanoporous structures, are presented with the example of Silicon. Similarly, in this chapter, the concept of convergence testing and the surface energies is also discussed with the example of silicon. All the DFT [90,99] energy calculations are carried out using the Program PWSCF v.4.3.2. This program is a part of open source QuantumESPRESSO suite [100] for quantum simulation of materials; and all the DFT calculations are spin-polarized within the projector augmented wave (PAW) approach [**?**]. The exchange correlation effects were modeled using the Perdew-Berke-Ernzerhof (PBE) generalized gradient approximation (GGA) approach [101]. The choice of pseudopotentials is same as that in various other important works. The Marzari-Vanderbilt method [102] was used as the smearing algorithm, the blocked Davidson iteration scheme [103] was chosen as the electron minimization algorithm and ions were updated using the conjugate gradient algorithm.

Convergence testing is done to decide the k-mesh size and the cut-off energy for the desired precision. Total energies (E_n) are physically quite meaningless in DFT, while energy differences (E_{diff}) are relevant. Generally, the energy resolution of 1meV/atom gives good approximation of the physical quantity under consideration.

$$E_{diff} = |E_{n+1} - E_n| \times 13.605698 \times \frac{1000}{N} \tag{3.2}$$

E_{n+1} and E_n (in Rydberg) are calculated DFT energies for two consecutive calculations from which, energy difference (E_{diff}) (in meV) is deduced. 1Ryd = 13.605698 eV. For silicon, N=8, the number of atoms in unit cell.

The following example is for oriented unit cell of silicon with the base oriented with the 001 family of planes of the conventional unit cell.

Initially, k-mesh size is worked out by energy calculations for different k-mesh sizes, such as $1 \times 1 \times 1$, $3 \times 3 \times 3$, $5 \times 5 \times 5$ and so on.

As observed from the k-pt convergence testing data, for the k-mesh size $7 \times 7 \times 7$, the precision acheived is < 1 meV and for the k-mesh size $9 \times 9 \times 9$, the precision acheived is < 0.1 meV

After deciding the k-point mesh size, convergence testing is done for basis set size.

Table 3.1: Convergence Testing for the k point Mesh Size

n	k-point	E_n (Ry)	time(s)	E_{diff} (meV/atom)
1	3	-373.80715258	15.71	-
2	5	-373.81570045	14.48	14.537467220
3	7	-373.81598675	26.12	0.486913917
4	9	-373.81600036	42.59	0.023146694
5	11	-373.81600565	66.07	0.008996768
6	13	-373.81600741	67.77	0.002993254
7	15	-373.81600616	137.38	0.002125890
8	17	-373.81600362	188.75	0.004319809
9	19	-373.81600242	251.40	0.002040855

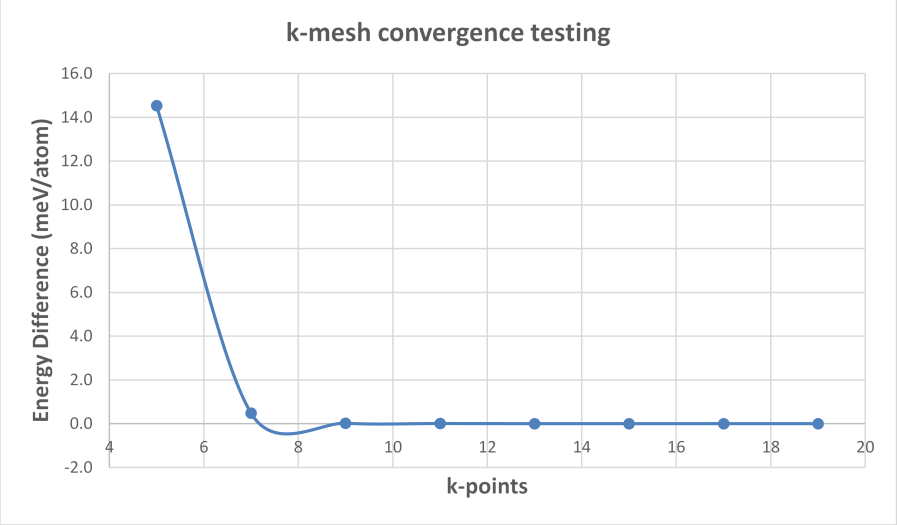

Figure 3.2: convergence testing for the k point mesh size

As expected, with the increase in basis set size or with larger cut off energy, the precision continues to improve. The setting of the basis set size depends upon the precision requirement.

As observed from the Tables 3.2 and 3.3 the computation time increases, with the improvement in precision by increasing k-mesh size and basis set size. Therefore, the accuracy of the calculations directly depends upon the availability of supercomputing hardware resource.

Due to the limited computing resource, the DFT calculations were performed with the plane wave cutoff energy of 80eV. The energies of all the calculations were converged to within 10^{-4} eV respectively. Γ-centered k-point meshes of $\frac{11}{a} \times \frac{11}{b} \times \frac{11}{c}$ and $\frac{5}{a} \times \frac{5}{b} \times \frac{1}{c}$ were used for OUC and the slab calculations respectively. Through a series of comprehensive convergence tests, it was determined that the value of vacuum and slab thicknesses were sufficient to ensure that the surface energies converged to within 0.02 Jm^{-2}.

The surface energy should be calculated for the 001, 110, 111 and 210 family of planes, as

Table 3.2: convergence testing for the basis set size

n	Basis set size (eV)	E_n (Ry)	time(s)	E_{diff} (meV/atom)
1	50	-373.81600036	42.59	-
2	60	-373.81602179	61.10	0.02143
3	70	-373.81603168	75.03	0.00989
4	80	-373.81604758	85.78	0.01590
5	90	-373.81607019	114.50	0.02261
6	100	-373.81607873	164.91	0.00854
7	110	-373.81608844	162.48	0.00971
8	120	-373.81610112	175.95	0.01268
9	130	-373.81610228	209.53	0.00116
10	140	-373.81610831	249.08	0.00603
11	150	-373.81611246	292.16	0.00415

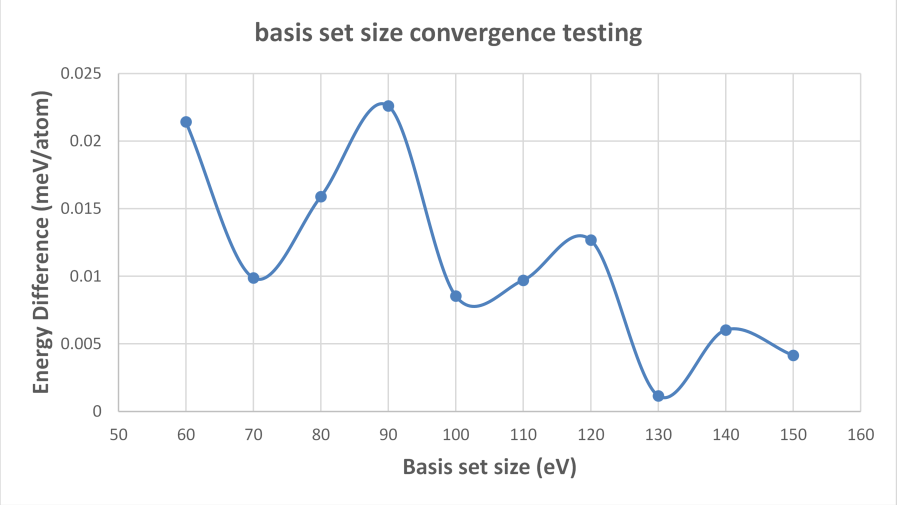

Figure 3.3: convergence testing for the basis set size

concluded in the previous chapter. For calculating the surface energy, slab model approach is used. The thickness of the bulk layers and the vacuum layer is an important consideration. The calculations were done by varying the thickness of the bulk layer and by keeping the vacuum layer size fixed.

The vacuum layer must be sufficiently large that the opposite surfaces do not interfere or interact. For the silicon slab, the thickness of vacuum is kept greater than 10Å as recommended in previous works [85, 86]. The convergence of thickness of vacuum layer is not tested due to the limitation of the computing hardware capability and this can be the part of future work.

In the real materials, due to the creation of the surface, the atoms at the surface are undercoordinated. Repositioning of the atoms of several layers minimize this effect. The atomic layers away from the surface maintain bulk structure configuration. This effect is mimicked

in the DFT energy calculations by observing the output file. For the DFT calculations of the slabs with the thicker bulk layer, some of the atomic layers at the center can be fixed [104]. This reduces the computation time without affecting the accuracy [104].

The results of the surface energy calculations for the (001) surface are presented in Fig. 3.4. The calculated surface energy is 2.1522 Jm^{-2}. and is converged to within $10^{-4} Jm^{-2}$.

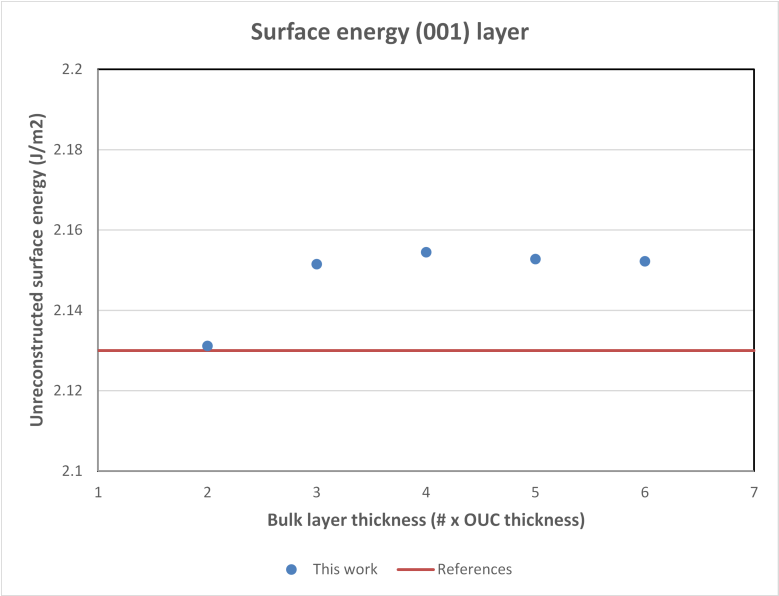

Figure 3.4: Surface energy for (001) surface.

Similarly the DFT energy calculations are performed for other surfaces (110), (111) and (210). Due to the limited available computation capability, only one surface energy calculation is performed for each surface. The initial bulk layer thickness of the slab is chosen to be three times OUC size and vacuum layer thickness two times OUC size which is greater than 10Å. Fig. 3.5, 3.6, 3.7 and 3.8 show side view of slab unit cells for different surfaces.

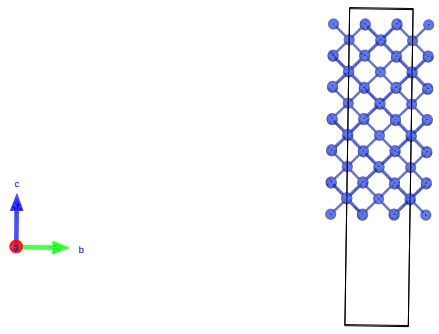

Figure 3.5: Bulk unit cell for (001) surface.

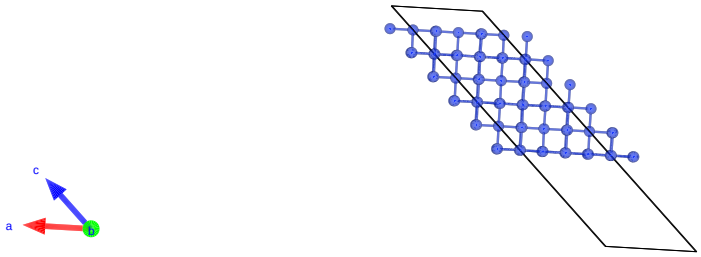

Figure 3.6: Bulk unit cell for (110) surface.

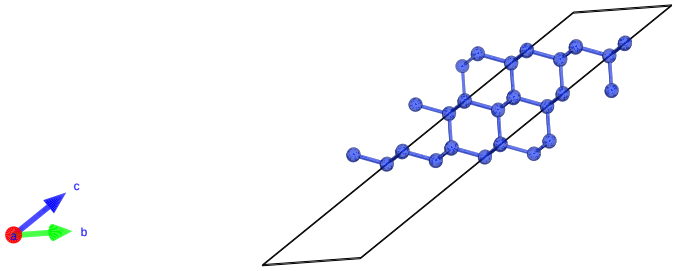

Figure 3.7: Bulk unit cell for (111) surface.

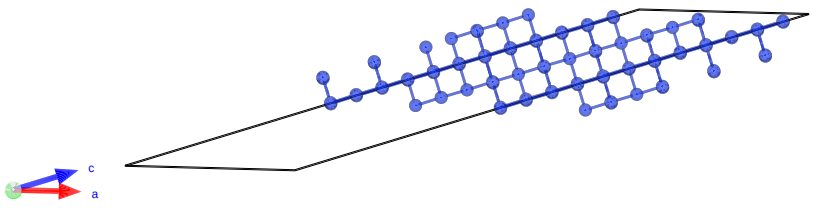

Figure 3.8: Bulk unit cell for (210) surface.

The results for the calculations are presented in the Table 3.3 and the comparison is drawn with the data available in literature.

Table 3.3: Results and Comparison.

Miller index	Unreconstructed		Reconstructed [105, 106]	Experiment [107]
	This work	Reference [86]		
(001)	2.1522(5)	2.13	1.28	1.23
(110)	1.7437	1.76	1.51	1.43
(111)	1.5781	1.57	1.30	1.36
(210)	1.5070	-	1.49	-

As mentioned in the Slab model section, in this work the surface energy calculations are performed for unreconstructed surfaces. The results of this work are quite consistent with the data of surface energy for such surfaces. However, the little difference is due to the difference in pseudopotentials and the DFT codes.

It is usually expected that the relaxed and the reconstructed surface energies are not much different, but the exceptions do exist, as seen from this example of silicon. The cleavage energy (term used for unreconstructed or relaxed surface energy) is much larger than the reconstructed surface energy. The cleavage of bulk along certain planes leaves the slab with asymmetric terminations on both the sides of the slab. These terminations have the unequal contribution in the surface energy leading to the cleavage energy. Surface energy for such materials is calculated by reconstructing the surfaces [85]. The problem of reconstruction of surfaces can be dealt in the future work.

From Table 3.3, it can also be concluded that the results of unconstructed surface energy calculations are much different from the experiment data. The case of silicon is quite an exception. Even though the calculated surface energy values, say for the metals, are quite consistent with the experimental data [86]. However, there is still some difference due to following reasons.

- There is a scope of uncertainty in the experimentally derived surface energies. The experimental values are extrapolations from the extreme values of the melting point [108]. There is a chance for the surface under study to get contaminated with elements such as oxygen. These limitations introduce errors in experimental data [109, 110].
- The limitations of the exchange correlation functions can be the cause of the further discrepancy [101]. This effect is slowly minimizing with the improvements of pseudopotentials and higher computing capabilities. In addition to this, the effect of VanderWaal forces is also not considered. This may introduce errors in surface energy calculations as in the case of graphene [111].
- Surface reconstructions may contribute to the difference in DFT calculations and the experimental data. Before performing DFT calculations, the surfaces are reconstructed

to maintain a good symmetry at the center of the slab. The missing row reconstructions are predicted by according the experimental and computational results [112].

In this chapter, after the brief introduction to surface energy, the methodology for calculating the surface energy using first principle calculations based on the DFT was presented. The important input parameters for DFT calculations, that affect the accuracy and precision of the results, were also presented with the help of convergence testing techniques. At the end, results of the calculations were compared with the data from the computational and experimental literature. This kind of study for the surface energy is very relevant for various applications as discussed in the introduction of this chapter. The focus of this work is to contribute towards the research of porous materials. For continuing the study further, the input data for the surface energy that is to be used should come from the calculations for reconstructed surfaces, as this data is consistent with the experimental results. The calculations for reconstructed surfaces did not form a part of this work, so the data is taken from computational reference databases [51,86]. Similarly, if anyone is working on the modeling of single crystal nanoporous materials and following the same methodology, it is advisable to start from the surface energy data from suitable databases.

Chapter 4

Modeling Nanoporous Materials with Minimum Spanning Tree Algorithm

4.1 Introduction to nanoporous materials

Nanoporous materials have been be known to the man from a very long time. There applications and the associated technology that is developed and accessed are either naturally occurring or man-made. Irrespective of the applications of nanoporous materials, the structure of nanoporous materials is a worth alook. It keeps us wondering what are the factors that make the properties of nanoporous materials so strange and wonderful. Porosity in the solids develops due to several routes - either it is the subtractive route such as electrochemical etching or the agglomeration of powders prepared by various techniques [113]. The porosity in the later route depends upon the size, shape and the packing of the constituting particles. Other than this, are the factors which are the focus of this study, that concern with the subtractive routes, such as - pore type, pore shape, pore size, pore volume and the surface area.

As mentioned in the Introduction Chapter of this work, before coming to the stage of modeling in any field of science, there is enough experimentation on the concerned phenomena. Theoreticians keep on modifying and developing the theories to inculcate new observations. The field of nanoporous materials may be quite old but still young in terms of the theory and the modeling. This is because of the scale that is under consideration. Several details are still missed out due to the limitations of the accuracy and precision of the experimental techniques. There are still many factors about which our knowledge is veiled and these affect our standard techniques of nanoporous materials' development. These inferences can be drawn from the following paragraphs.

Hereafter, the literature survey is pertaining to nanoporous silicon only. The experimental study of the structure of the nanoporous materials is done on the samples that are ultra thin (10-100 nm) in thickness [114]. Porosity is introduced in the materials by suitable etching

techniques, esp. via electrochemical etching. The factors that are studied are as under:

- **Pore type** An etch pit is called a pore when its depth on the sample exceeds its width. Depending upon the time of etching, pores grow. The different type of pores that can occur in the material, such as blind or dead end pores, interconnected or branched pores, totally isolated or closed pores or through pores as shown in Fig. 4.1. The occurrence of the different types of the pores is due to different behavior of different materials for same etching conditions, or change in etching conditions due to change of parameters of etching technique, or change of technique itself.

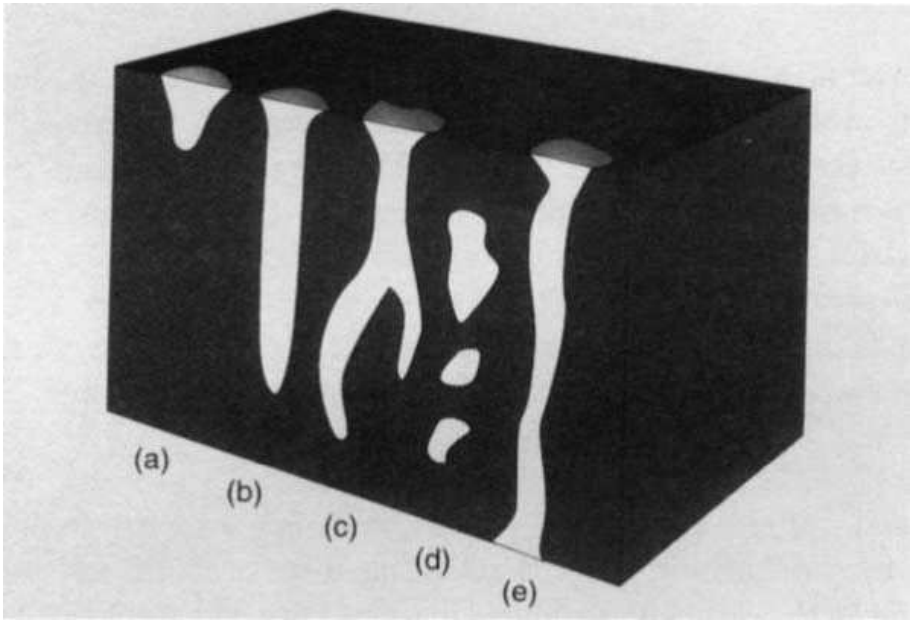

Figure 4.1: Type of pores (a,b)blind or dead end (c) interconnected or branched (d) isolated or closed (e) through pores [115]

- **Pore shape** Depending upon the time of etching or due to a different lattice direction, the pore shape may get altered. As observed, pores on the surface are much wider compared to those present in the underlying layers [117]. The effect of etchant on the material is an important consideration that needs to be understood. The different shapes of pores that are reported are cylindrical, ink-bottle, cuboidal or slit and triangular or pyramidal [116] as shown in Fig 4.2.

- **Pore size** Pore size affects the adsorption properties of the nanoporous materials. Though the cohesive forces between the solid porous materials also affect this relationship, however, the pore size seriously alters the adsorption behavior. Therefore, depending upon the different adsorption characteristics of the pores [118], IUPAC has categorized pores based on their size, as is shown in Table 4.1

  Pore size has the precise meaning when the geometry of the shape of the pore is

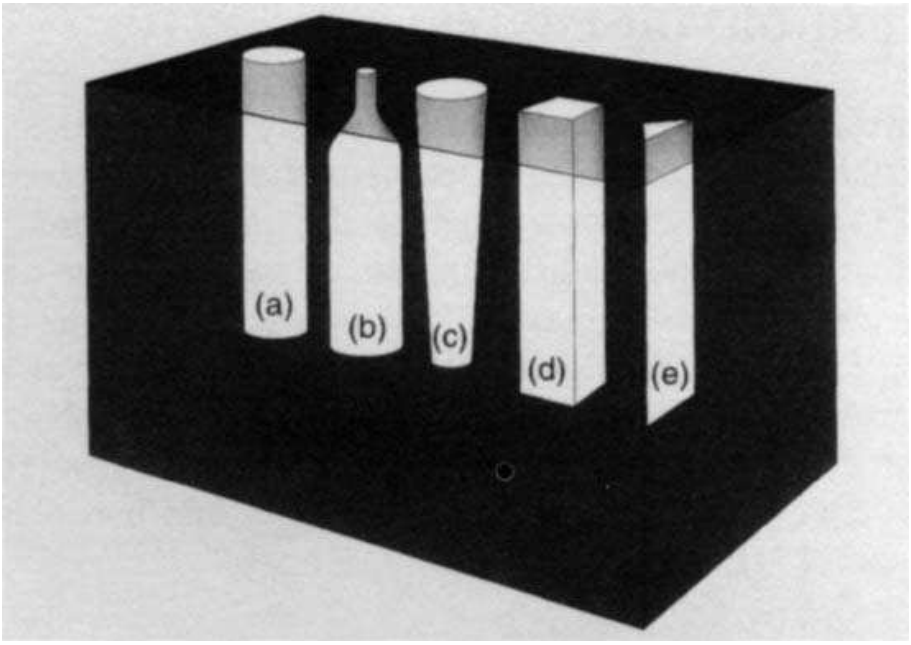

Figure 4.2: Pore shapes (a) cylindrical, (b) ink-bottle, (c) cuboidal or slit and (e) triangular or pyramidal. [115]

Table 4.1: IUPAC classification of pore size.

Pore width (in nm)	Type of pore
≤ 2	micro
2 - 50	meso
> 50	macro

known and well defined. For low porous microporous, sometimes mesoporous and microporous, the shape is generally not defined properly.

- **Pore volume or void content** The apparent volume of the sample allocated to the pores as found by the experimental technique may be defined as porosity [119]. The porosity of closed pores is not considered by the present experimental techniques. Depending upon the void content, the porosity can be characterized as shown in the Table 4.2.

Table 4.2: Classification of porosity.

Void content %	Porosity level	Potential application areas for nanoporous Si [115]
0 - 30	low	wafer bonding, tissue bonding and microcapacitors
30 - 70	medium	sensors, silicon insulators and micromaching
70 - 100	high	non-linear optics, LEDs and anti-reflective coatings

- **Surface area** In relation to nanoporous materials, the term surface area is attributed to the internal surface area due to the pores that are accessible by various experimental techniques. It may be up to few m^2 per gram for macroporous materials or thousands of m^2 per gram for microporous materials.

The knowledge of the parameters, that affect the microstructure of the materials, helps in developing materials with very useful properties. The porosity parameter does not give any information of the microstructure of the material. Information of the pore size, shape, and its distribution helps in developing the knowledge of the microstructure and developing monocrystalline nanoporous materials with desired properties. There has been a very limited comprehensive study of the pore networks for monocrystalline porous materials due to the insufficient data. One reason is due to different experimental techniques used for analyzing the pore sizes. Either these are critical and costly techniques or require elaborate modeling or large porous volume to deduce quantitative results. The other reason for the lack of data is the shift of interest of researchers. Either the analysis is done for composite nanoporous structures in which pores are filled with certain gas or liquid, or the crystallite formations which is the cause of luminescence in nanoporous Silicon. The study in this work is limited to monocrystalline nanoporous materials. The future work may be around nanoporous composite materials and their applications.

4.2 Modelling Nanoporous Materials

There are a number of factors, as mentioned in the preceding paragraphs, that affect the morphology of the nanoporous materials. Modeling of all these factors with limited understanding of the experimental results makes the job very cumbersome and confusing. However, with the systematic honest attempt, a way can be paved towards relic of the knowledge. Though this is not a new problem of modeling random nanoporous materials, several attempts have been made before [34, 120]. These have their own glories and limitations [34, 120].

4.2.1 Brief review of the challenge

Nanoporous materials are porous structures consisting of regular organic or inorganic framework [121]. The material properties of the nanoporous materials depend upon several parameters, such as:

- **Very large surface area**

  Nanoporous materials have very large internal surface area due to the presence of nano-sized pores, exceeding 5000 m^2g^{-1} in the most porous materials [39]. Large active surface area adsorbs ions and molecules and facilitates the nanoscale phenomena, useful in applications like heterogeneous catalysis [37] and gas storage [39].

- **Effects of quantum confinement**

  Quantum confinement is the phenomena due to which electronic and optical properties of nanoporous materials deviate substantially from the bulk material. The phenomena occur when the size of the material is in close proximation of the de Broglie wavelength of the electron wave function [122]. Quantum sieving effect is one of the nanoporous

application which allows molecular separation, as lighter atoms have different diffusion rates in narrow micropores [38].

- **Presence of certain active sites**

  The presence of certain active sites on the large internal surface area of the nanoporous materials may lead to preferential adsorption of ions or atoms. This facilitates in heterogeneous catalytic reactions [37] or gas storage and separation applications [38]. For the preferential adsorption of reaction species sometimes certain guest elements may be introduced to the large internal surface area of the nanoporous materials [37].

Considering these factors, the properties of nanoporous materials can be tailor-made to suit several applications, such as heterogeneous catalysis [37], biomedical imaging and drug delivery [40], gas storage [38, 39], membrane filtration [38], electrochemical supercapacitors [42], photovoltaic applications [41], photo luminescent applications, etc. As discussed in chapter 1, the properties of the materials depend upon the composition and microstructure of the material. The evolution path of the microstructure depends upon the lattice defects in the material and the evolution direction of the microstructure depends upon thermodynamics parameters such as temperature, pressure and so forth. The material phenomena can be explained by the help of some theory or a model. Based on the developed model, numerical calculations or simulations can be performed. The aims of the simulations are

- To develop better insight of physical principles that control the microstructure evolution
- To develop microstructure property relations
- To probe conditions that are not accessible for experimentation
- To predict the results before experimentation

The nanoporous materials may seem to be chaotic and random and show characteristic complex structure. But by proper modeling, the different parts may be related to one another, in a non-random way with identifiable regularities and recurring patterns. This is the theme of this work.

In the present work, by comparing the different applications of the nanoporous materials, some common characteristics of the nanoporous materials are realized as shown in Fig. 4.3. The common characteristics can act as modeling parameters for the modeling of random nanoporous materials.

The objective of the work is to present a generalized algorithm for the modeling of random nanoporous crystalline materials is initiated. Based on the modeling parameters, i.e. shape and size of pores and the composition of the materials, the random distribution porous network is realized. This porous network seems absurd if compared with the experimental data because the nanoporous growth environment also affects the porous network. Therefore,

Table 4.3: Modelling Parameters

Nanoporous materials applications	**Ref**	**Modelling Parameters**				
		Pore size	Pore shape	Bulk composition	Surface composition	active sites
Heterogeneous Catalysis	[37]	✔	✔	✔	✔	✔
Biomedical imaging and Drug delivery	[40]	✔	✔	✘	✔	✔
Electrochemical capacitors	[42]	✔	✔	✔	✔	✘
Gas Storage	[38]	✔	✔	✔	✔	✔
Photovoltaic applications	[41]	✔	✔	✔	✔	✘

the next step is to inculcate the environment dependent or thermodynamic parameters such as temperature, pressure and so forth. The environment dependent parameters are not yet included in the study and once that is done, the results of the proposed algorithm can be directly compared with the experimental data.

4.2.2 Graph theory approach

The novelty of this work lies in introducing the graph theory to the material science. Graph theory is the branch of mathematics, that describes networks at the most elementary level, as the set of nodes and links or edges [123]. In the present work, the application of graph theory is extended to the modeling of porous networks of nanoporous materials. Nanoporous material parameters, such as pore size, pore shape, bulk and surface compositions and presence of active sites, can be dealt in a systematic way. Other well-known applications of graph theory deal with the problems of social networks [124], transportation networks [124], neural networks [124] and much more [125].

In graph theory, a network is described as the set of nodes and edges. The nodes are connected by the edges and choice of connections or edges between several nodes is based on some rule [123, 124]. That rule decides the weight of an edge. In graph theory, a tree is defined as an acyclic graph. A minimum spanning tree (MST) of a connected weighted graph is the spanning tree of this graph that minimizes the sum of the weights of the edges included in the tree [123, 124]. There are two main algorithms for the development of MST, i.e. Kruskal's algorithm [126] and Prim's algorithm [127].

In the present work, the modeling of porous networks is done based on the Kruskal's algorithm. The steps for the Kruskal's algorithm are as follows.

- Sort the edges of the weighted graph from lowest to highest weights

- Sorted edges according to the weight are added to the tree in ascending order; avoiding cycles

The key inputs for the Kruskal's algorithm are starting nodes per volume and weight of the edges based on some rule [128]. The nanoporous modeling parameters, mentioned in Fig. 4.3, help to specify the key inputs for the Kruskal's algorithm.

Initially, it is assumed the weight of the edge depends on the size of the pore, the direction of growth of the pore and its length. This assumption is supported by the literature that reports that different pore sizes may have specific shapes and also depend upon growth direction of the pore [116]. It can also be easily imagined during the pore formation; certain surfaces are created parallel to edge direction and energy is spent by the environment during pore formation due to some underlying phenomena [76,116] as shown in Fig 4.3. The idea of the presence of surfaces leads us to the concept of surface energy. It is the energy required for the cleavage of lattice plane to create the surface [86] and it varies along different lattice planes.

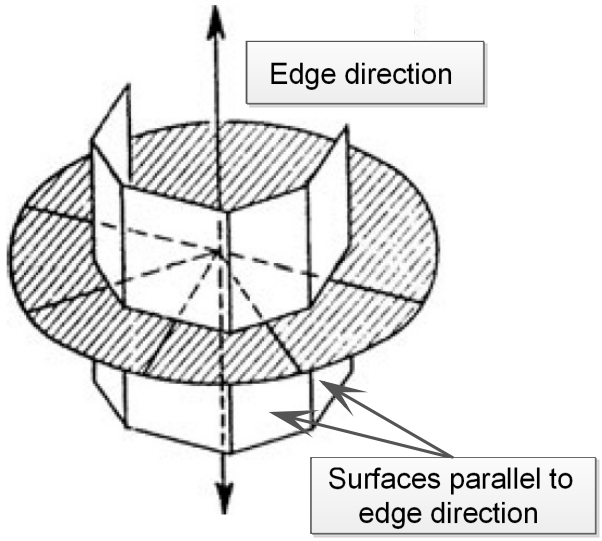

Figure 4.3: Surfaces are created parallel to the edge direction.

The methods for choosing the specific plane families for any edge direction and the methods for calculating surface energy along these planes are elaborately discussed in previous Chapters 2 and 3.

From the discussion in these chapters, it can be also be concluded that in the real world, most of the crystalline inorganic materials are anisotropic. As the surface energy shows variations

- Along different orientation of the crystal surface, depending upon the crystal structure of crystalline material
- For different bulk and surface compositions

From the above arguments and the discussion, surface energy seems to be a wise choice for the weight parameter rule of the Kruskal's algorithm. As mentioned before, other than the surface energy, pore size is another parameter contributing towards the weight. This helps is deciding pore shape and even contribute towards the family of plane selection for calculating surface energy. This topic is not dealt here due to the limitation of resources.

Thus weight parameter of the Kruskal's algorithm becomes the function of surface energies and the pore size, as shown with the example of Silicon.

$$wt_{001} = f(E^{001}_{surf}, E^{110}_{surf}, pore\_size)$$
$$wt_{110} = f(E^{001}_{surf}, E^{110}_{surf}, E^{111}_{surf}, pore\_size)$$
$$wt_{111} = f(E^{110}_{surf}, E^{211}_{surf}, pore\_size)$$

Similarly, with the addition of other relevant parameters, the proper weight function can be evolved which is ultimately comparable with the experimental data. With the evolvement of weight function, our knowledge of the nanoporous materials parameters and their relationship also improves.

4.2.3 Steps for the Proposed Algorithm for the Modeling of Random Nanoporous Material

Based on the steps of the proposed algorithm, a C-language code was developed to design the skeleton network of the pores in a porous material. The steps for the development of the C-code are presented below.

- Initialize the starting nodes randomly in the system volume. The distribution of the nodes along certain coordinate axes can also be varied. The ratio of the number of starting nodes to system volume size is assumed to depend upon the unit cell length such that the average distance between two nodes is around few lattice unit lengths. The starting nodes affect the distribution of pores and the net porosity of the material.
- Make the verlet list of all the nodes. Verlet list is the list of nearest neighbors up to a certain fixed distance [129]. Choice of the fixed distance depends upon the distance between the starting nodes. This step considerably reduces the computation time.
- Weight is calculated for each node forming its pair with every other node in its verlet list. This step uses the concept of possible favorable directions and the associated surface energies.
- The pair weights are sorted from smallest to largest. Several sorting algorithms are available in the literature. Bubble sort algorithm is used in the present work. The computation time also depends upon the choice of sorting algorithm.

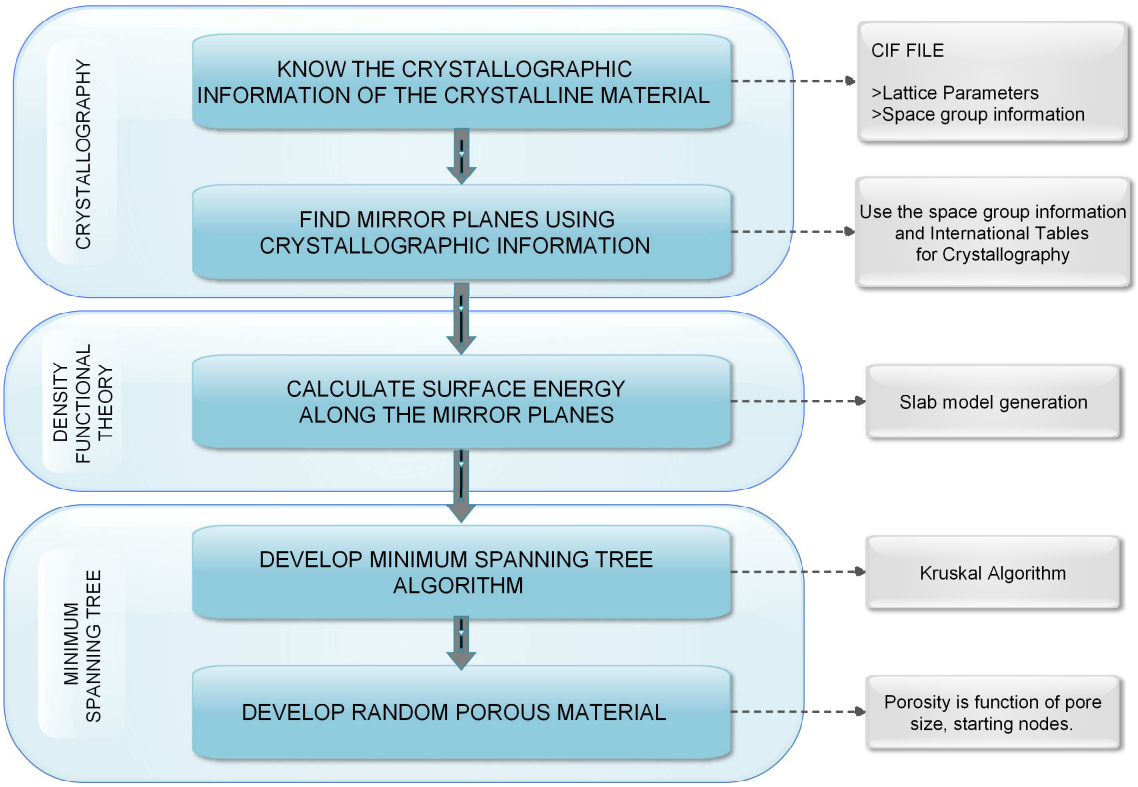

Figure 4.4: Steps for the Proposed Algorithm for the Modeling of Random Nanoporous Material.

- The porous network is created by using the minimum spanning tree algorithms. The sorted list of weights and associated node number is used to create a joined network of pores, such that cyclic connections are avoided
- All the nodes can be connected to form a single tree, but it is not advisable as the distance towards the end becomes very large compared to the average distance between the nodes. description

The C-language code to design the skeleton network of the pores in a porous material is presented below.

```
#include<stdio.h>
#include<math.h>
#include<stdlib.h>
#include<time.h>
#define PI 3.141592653589793
#define RR 1
float distance(int size,float x1,float y1,float z1,float x2,float y2,float z2)
{
float dx,dy,dz,dist;
dx=x2-x1;
```

```
dy=y2-y1;
dz=z2-z1;

if(dx>size/2)
dx=dx-size;
else if(dx<-size/2)
dx=dx+size;

if(dy>size/2)
dy=dy-size;
else if(dy<-size/2)
dy=dy+size;

if(dz>size/2)
dz=dz-size;
else if(dz<-size/2)
dz=dz+size;

dist=sqrt(dx*dx+dy*dy+dz*dz);
return dist; }

void weight(int size,float x1,float y1,float z1,float x2,float y2,float z2,
float *wt, int *dir){
float dx,dy,dz,dist,th,phi;
float th1,phi1;
int i;
dx=x2-x1;
dy=y2-y1;
dz=z2-z1;

if(dx>size/2)
dx=dx-size;
else if(dx<-size/2)
dx=dx+size;

if(dy>size/2)
dy=dy-size;
else if(dy<-size/2)
```

```
dy=dy+size;

if(dz>size/2)
dz=dz-size;
else if(dz<-size/2)
dz=dz+size;

dist=sqrt(dx*dx+dy*dy+dz*dz);
th=atan2(dz,sqrt(pow(dx,2)+pow(dy,2)));              //vertical angle
phi=atan2(dy,dx);                                    //horizontal angle

printf("\n%f %f",(180/PI)*th,(180/PI)*phi);

float phip[26] = {0,PI/2,0,PI/4,3*PI/4,0,PI,PI/2,-PI/2,PI/4,3*PI/4,-PI/4,
-3*PI/4, PI,0,-3*PI/4,-PI/4,0, PI,PI/2,-PI/2, PI/4,3*PI/4,-PI/4, -3*PI/4};
float thp[26]={0,0,PI/2,0,0,PI/4,PI/4,PI/4,PI/4, PI/4,PI/4,PI/4,PI/4,0,0,
-PI/2,0,0,-PI/4,-PI/4,-PI/4,-PI/4,-PI/4,-PI/4,-PI/4,-PI/4};
//0----->100                        //13----->-100
//1----->010                        //14----->0-10
//2----->001                        //15----->00-1
//3----->110                        //16----->1-10
//4----->-110                       //17----->-1-10
//5----->101                        //18----->10-1
//6----->-101                       //19----->-10-1
//7----->011                        //20----->01-1
//8----->0-11                       //21----->0-1-1
//9----->111                        //22----->11-1
//10---->-111                       //23----->-111
//11---->-1-11                      //24----->-1-1-1
//12---->1-11                       //25----->1-1-1
float ener[26]={1.395,1.395,1.395,1.363333,1.363333,1.363333,1.363333,1.363333,
1.363333,1.395,1.395,1.395,1.395,1.395,1.395,1.395,1.363333,1.363333,1.363333,
1.363333,1.363333,1.363333,1.395,1.395,1.395,1.395},ww[26];
//ASSUMPTION (without proof)
//surface energy of {001}= (ener(001)+ener(110))/2
//surface energy of {110}= (ener(001)+ener(110)+ener(111))/3
//surface energy of (111)= (ener(111)+ener(210))/2
for(i=0;i<26;i++){
```

```
ww[i]=(180/PI)*acos(sin(phi)*sin(phip[i])+cos(phi)*cos(phip[i])*cos(th-thp[i]));}

for(i=0;i<26;i++){
if(ww[i]<=30){
*wt=2*PI*RR*dist*ener[i]*ww[i];
dir+[i]++;
break;}}
}
void swap(float *xp, float *yp)
{
float temp = *xp;
*xp = *yp;
*yp = temp;}

void bubbleSort(float no1[], float no2[], float arr[], int n)
{
int i, j;
for (i = 0; i < n-1; i++)
for (j = 0; j < n-i-1; j++)
if (arr[j] > arr[j+1]){
swap(&arr[j], &arr[j+1]);
swap(&no1[j], &no1[j+1]);
swap(&no2[j], &no2[j+1]);
}}

int main()
{
int size=10,n=100,i,j,k;
float r_cut=30;
float xr[n],yr[n],zr[n];
int **verl;
float dist,wt;
float **wgt;
FILE *fp1;
fp1=fopen("enteries.txt","w+");
int cnt;
int gp[n],dir[26];
srand((unsigned)time(NULL));
```

```
for(i=0;i<n;i++){                                  //declaring random numbers
xr[i]=size*(rand()%RAND_MAX/(float)RAND_MAX);
yr[i]=size*(rand()%RAND_MAX/(float)RAND_MAX);
zr[i]=size*(rand()%RAND_MAX/(float)RAND_MAX); }

verl = (int **)malloc(n*sizeof(int *));        //initialize verlet list
for(i=0;i<n;i++)
verl[i]= (int *)malloc(n*sizeof(int));

for(i=0;i<n;i++)                                  //making verlet list
for(j=0;j<n;j++)
verl[i][j]=-1;

for(i=0;i<n;i++){
k=0;
for(j=0;j<n;j++){
if(i!=j){
dist=distance(size,xr[i],yr[i],zr[i],xr[j],yr[j],zr[j]);
printf("%d %f\n",i,dist);
if(dist<r_cut){
verl[i][k]=j;
k++;}}}}

for(i=0;i<n;i++){ printf("\n");
for(j=0;j<n;j++)
printf("%d\t",verl[i][j]);}

for(i=0;i<26;i++)
dir[i]=0;

cnt=0;                                            //calculating wts
for(i=0;i<n;i++){j=0;
k=verl[i][j];
while(k!=-1){
if(i<=k){
weight(size,xr[i],yr[i],zr[i],xr[k],yr[k],zr[k],&wt,dir);
fprintf(fp1,"%d %d %f\n",i,k,wt);
```

```
cnt++;}
j++;
k=verl[i][j];  }}

fclose(fp1);
printf("\n%d",cnt);

wgt = (float **)malloc(cnt*sizeof(float *));    //initialize weight list
for(i=0;i<cnt;i++)
wgt[i]= (float *)malloc(4*sizeof(float));

fp1=fopen("enteries.txt","r+");
if(fp1==NULL){
printf("could not open data file");
exit(-1);}

for(i=0;i<cnt;i++){
fscanf(fp1,"%f %f %f\n",&wgt[i][1],&wgt[i][2],&wgt[i][3]);
wgt[i][0]=i+1;}

for(i=0;i<cnt;i++){printf("\n");
for(j=0;j<4;j++)
printf("%f\t",wgt[i][j]);}

j=0;
for(i=0;i<26;i++){
printf("\n%d %d",i,dir[i]);
j=j+dir[i];}

fclose(fp1);
printf("\n%d",j);

float list[cnt],temp;
float no1[cnt],no2[cnt];
for(i=0;i<cnt;i++){
no1[i]=wgt[i][1];
no2[i]=wgt[i][2];
list[i]=wgt[i][3];}
```

```
bubbleSort(no1,no2,list,cnt);

for(i=0;i<cnt;i++)
printf("\n%d %f %f %f",i,no1[i],no2[i],list[i]);
//intialising group no for each node
for(i=0;i<n;i++)
gp[i]=0;

int edge[cnt],a,newgp=1;
for(i=0;i<cnt;i++)
edge[i]=0;

for(i=0;i<cnt;i++){
if(gp[(int)no1[i]]==0){
if(gp[(int)no2[i]]==0){
edge[i]=1;
gp[(int)no1[i]]=gp[(int)no2[i]]=newgp++;
printf("\n%d %d",gp[(int)no1[i]],gp[(int)no2[i]]);}
else{
edge[i]=1;
gp[(int)no1[i]]=gp[(int)no2[i]];}}
else{
if(gp[(int)no2[i]]==0){
edge[i]=1;
gp[(int)no2[i]]=gp[(int)no1[i]];}
else{
if(gp[(int)no1[i]]!=gp[(int)no2[i]]){
if(gp[(int)no1[i]]<gp[(int)no2[i]]){
edge[i]=1;
a=gp[(int)no2[i]];
for(j=0;j<n;j++)
if(gp[j]==a)
gp[j]=gp[(int)no1[i]];}
else{
edge[i]=1;
a=gp[(int)no1[i]];
for(j=0;j<n;j++)
if(gp[j]==a)
```

```
gp[j]=gp[(int)no2[i]];}}}}}
printf("\n\n'ruskal edges between pts and resp. wts");
for(i=0;i<cnt;i++)
if(edge[i]==1)
printf("\n%d %f %f %f",i,no1[i],no2[i],list[i]);
return 0;}
```

The porous microstructure using the above C-code is presented in Fig. 4.5.

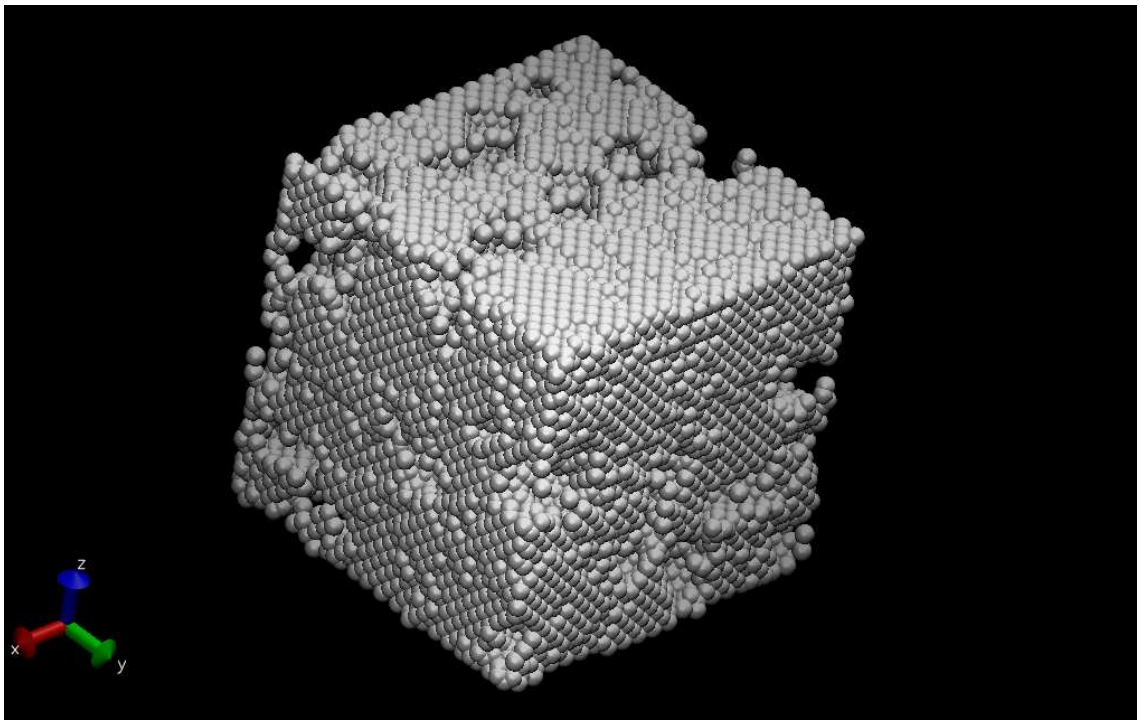

Figure 4.5: Developed silicon nanocluster. The image is produced using VMD software [130]

The success of the proposed algorithm depends upon how well the input parameters are explored and inculcated in the algorithm. At the present stage with the incomplete and inadequate knowledge of the input parameters, the algorithm is still in the development phase. Therefore, the results of the proposed algorithm cannot be compared with any experimental data. The present work is quite eclectic and can serve as a preliminary study for the modeling of random nanoporous materials.

4.3 Future work and other possibilities

The modeling of random nanoporous materials, no doubt, is a multifarious problem. In this preliminary work, the solution to this problem has been initiated and just need to be extended to its full multitudinous.

- To study the change in surface energy in the presence of guest elements or foreign impurities on the surface.

Active sites are one of the important modeling parameters listed in Table 4.3. However, due to limited resources, this parameter is not worked upon here. Presence of active sites significantly affects the characteristics of nanoporous materials.

- To identify pore shapes along different directions and inculcating the effect of foreign elements.

  This study is useful for improving the presented work for predicting the pore network distribution. Considering the thermodynamic parameters of pore formation and use of molecular dynamics can help to converge this study for designing materials for microfluidics [131] and other related applications.

- Introducing percolation models [132]

  The number of nodes per unit volume is a key input for the Kruskal's algorithm. However, it is not addressed in this study. The percolation models can help in controlling the material porosity by appropriately defining the number of nodes per unit volume.

- Introducing molecular dynamics

  The molecular dynamics helps in understanding the dynamics and stability of the system. By using DFT, very limited number of atoms can be dealt but using MD, thousands of atoms can be handled; therefore, MD can directly aid towards the development of nanoporous materials. The large microstructure can be developed and compared with experimental data. This method can be used if proper set of force-fields are available for the addressed material. Say for silicon, the available force-fields [133] are not suitable for the different nanoporous system requirements.

- Studying and estimating material properties of the nanoporous structure

  In this work, nanoporous materials applications are not directly addressed. As, every application is a set of new phenomena involving several computational challenges. There is a need for the development of better computational methodologies for dealing with the challenges. The existing theories can be improved if the theoretical results are in correlation with the experimental data. With the improvement of information, the new possibilities with the nanoporous materials can be predicted and developed.

- Quantifying the similarity of pore geometry in nanoporous materials and prediction of possible applications

  The field of topological data analysis has been recently introduced to the field of material science [134]. This novel approach has several opportunities.

These studies can serve as benchmarks for a single model project that has the potential to improve the existing materials properties and predict new materials.

Appendix A

Space groups and plane groups

This part presents the Space group information chart, for the unit cell having $Fd\bar{3}m$ symmetry, from *International Tables of Crystallography- Vol A* [67].

The plane groups along special projections directions can be deduced from the Symmetry of Special projections block. The deduced information is shown in Table A.1.

Table A.1: Plane group symmetry along speical projection directions for Si unit cell.

Special Projection Directions	Plane groups	References
001	p4mm	[68]
111	p6mm	[69]
110	c2mm	[70]

The respective plane groups symmetry information charts are also presented. These are also included from *International Tables of Crystallography- Vol A*.

International Tables for Crystallography (2006). Vol. A, Space group 227, pp. 696–703.

$F\,d\,\bar{3}\,m$ O_h^7 $m\bar{3}m$ Cubic

No. 227 $F\ 4_1/d\ \bar{3}\ 2/m$ Patterson symmetry $F\,m\,\bar{3}\,m$

ORIGIN CHOICE 1

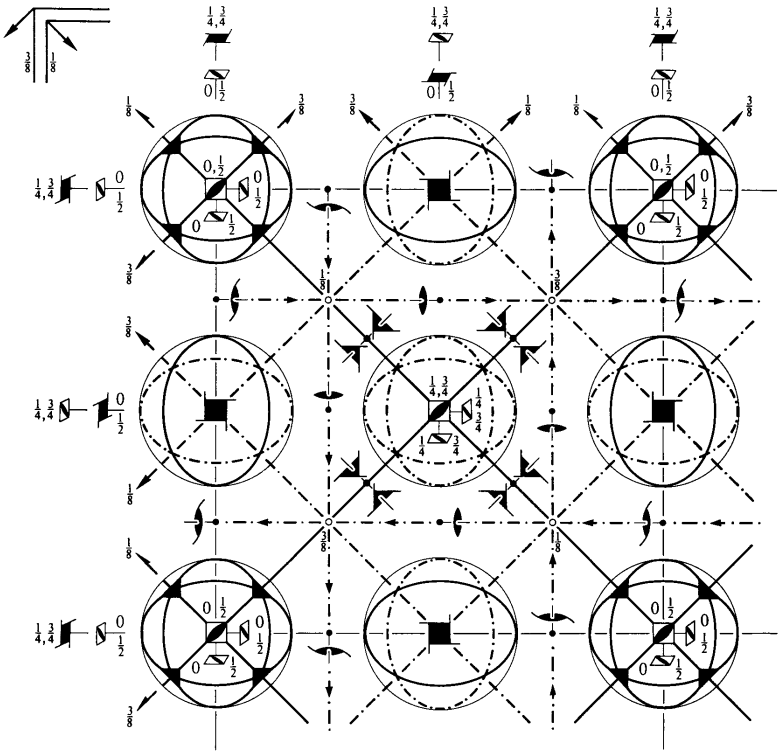

Upper left quadrant only

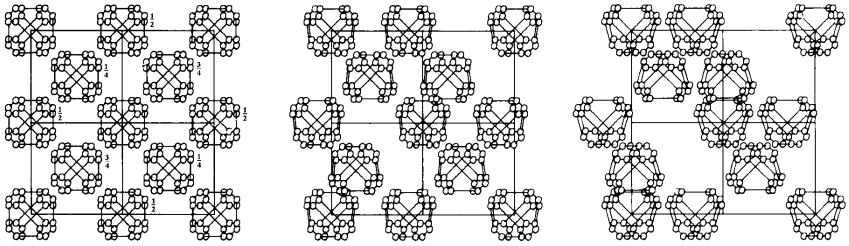

Origin at $\bar{4}\,3m$, at $-\frac{1}{8},-\frac{1}{8},-\frac{1}{8}$ from centre $(\bar{3}\,m)$

Asymmetric unit $0 \le x \le \frac{1}{2}$; $0 \le y \le \frac{1}{8}$; $-\frac{1}{8} \le z \le \frac{1}{8}$; $y \le \min(\frac{1}{2}-x,x)$; $-y \le z \le y$

Vertices $0,0,0$ $\frac{1}{2},0,0$ $\frac{3}{8},\frac{1}{8},\frac{1}{8}$ $\frac{1}{8},\frac{1}{8},\frac{1}{8}$ $\frac{3}{8},\frac{1}{8},-\frac{1}{8}$ $\frac{1}{8},\frac{1}{8},-\frac{1}{8}$

Symmetry operations

(*given on page* 699)

Generators selected (1); $t(1,0,0)$; $t(0,1,0)$; $t(0,0,1)$; $t(0,\frac{1}{2},\frac{1}{2})$; $t(\frac{1}{2},0,\frac{1}{2})$; (2); (3); (5); (13); (25)

Positions

Multiplicity, Wyckoff letter, Site symmetry			Coordinates $(0,0,0)+$	$(0,\frac{1}{2},\frac{1}{2})+$	$(\frac{1}{2},0,\frac{1}{2})+$	$(\frac{1}{2},\frac{1}{2},0)+$	Reflection conditions
							h,k,l permutable
							General:
192	i	1	(1) x,y,z	(2) $\bar{x},\bar{y}+\frac{1}{2},z+\frac{1}{2}$	(3) $\bar{x}+\frac{1}{2},y+\frac{1}{2},\bar{z}$	(4) $x+\frac{1}{2},\bar{y},\bar{z}+\frac{1}{2}$	hkl : $h+k=2n$ and $h+l,k+l=2n$
			(5) z,x,y	(6) $z+\frac{1}{2},\bar{x},\bar{y}+\frac{1}{2}$	(7) $\bar{z},\bar{x}+\frac{1}{2},y+\frac{1}{2}$	(8) $\bar{z}+\frac{1}{2},x+\frac{1}{2},\bar{y}$	$0kl$: $k+l=4n$ and $k,l=2n$
			(9) y,z,x	(10) $\bar{y}+\frac{1}{2},z+\frac{1}{2},\bar{x}$	(11) $y+\frac{1}{2},\bar{z},\bar{x}+\frac{1}{2}$	(12) $\bar{y},\bar{z}+\frac{1}{2},x+\frac{1}{2}$	hhl : $h+l=2n$
			(13) $y+\frac{3}{4},x+\frac{1}{4},\bar{z}+\frac{3}{4}$	(14) $\bar{y}+\frac{1}{4},\bar{x}+\frac{1}{4},\bar{z}+\frac{1}{4}$	(15) $y+\frac{1}{4},\bar{x}+\frac{3}{4},z+\frac{3}{4}$	(16) $\bar{y}+\frac{3}{4},x+\frac{3}{4},z+\frac{1}{4}$	$h00$: $h=4n$
			(17) $x+\frac{3}{4},z+\frac{1}{4},\bar{y}+\frac{3}{4}$	(18) $\bar{x}+\frac{3}{4},z+\frac{3}{4},y+\frac{1}{4}$	(19) $\bar{x}+\frac{1}{4},\bar{z}+\frac{1}{4},\bar{y}+\frac{1}{4}$	(20) $x+\frac{1}{4},\bar{z}+\frac{3}{4},y+\frac{3}{4}$	
			(21) $z+\frac{3}{4},y+\frac{1}{4},\bar{x}+\frac{3}{4}$	(22) $z+\frac{1}{4},\bar{y}+\frac{3}{4},x+\frac{3}{4}$	(23) $\bar{z}+\frac{3}{4},y+\frac{3}{4},x+\frac{1}{4}$	(24) $\bar{z}+\frac{1}{4},\bar{y}+\frac{1}{4},\bar{x}+\frac{1}{4}$	
			(25) $\bar{x}+\frac{1}{4},\bar{y}+\frac{1}{4},\bar{z}+\frac{1}{4}$	(26) $x+\frac{1}{4},y+\frac{3}{4},\bar{z}+\frac{3}{4}$	(27) $x+\frac{3}{4},\bar{y}+\frac{3}{4},z+\frac{1}{4}$	(28) $\bar{x}+\frac{3}{4},y+\frac{1}{4},z+\frac{3}{4}$	
			(29) $\bar{z}+\frac{1}{4},\bar{x}+\frac{1}{4},\bar{y}+\frac{1}{4}$	(30) $\bar{z}+\frac{3}{4},x+\frac{1}{4},y+\frac{3}{4}$	(31) $z+\frac{1}{4},x+\frac{3}{4},\bar{y}+\frac{3}{4}$	(32) $z+\frac{3}{4},\bar{x}+\frac{3}{4},y+\frac{1}{4}$	
			(33) $\bar{y}+\frac{1}{4},\bar{z}+\frac{1}{4},\bar{x}+\frac{1}{4}$	(34) $y+\frac{3}{4},\bar{z}+\frac{3}{4},x+\frac{1}{4}$	(35) $\bar{y}+\frac{3}{4},z+\frac{1}{4},x+\frac{3}{4}$	(36) $y+\frac{1}{4},z+\frac{3}{4},\bar{x}+\frac{3}{4}$	
			(37) $\bar{y}+\frac{1}{2},\bar{x},z+\frac{1}{2}$	(38) y,x,z	(39) $\bar{y},x+\frac{1}{2},\bar{z}+\frac{1}{2}$	(40) $y+\frac{1}{2},\bar{x}+\frac{1}{2},\bar{z}$	
			(41) $\bar{x}+\frac{1}{2},\bar{z},y+\frac{1}{2}$	(42) $x+\frac{1}{2},\bar{z}+\frac{1}{2},\bar{y}$	(43) x,z,y	(44) $\bar{x},z+\frac{1}{2},\bar{y}+\frac{1}{2}$	
			(45) $\bar{z}+\frac{1}{2},\bar{y},x+\frac{1}{2}$	(46) $\bar{z},y+\frac{1}{2},\bar{x}+\frac{1}{2}$	(47) $z+\frac{1}{2},\bar{y}+\frac{1}{2},\bar{x}$	(48) z,y,x	
							Special: as above, plus
96	h	. . 2	$\frac{1}{8},y,\bar{y}+\frac{1}{4}$	$\frac{7}{8},\bar{y}+\frac{1}{2},\bar{y}+\frac{3}{4}$	$\frac{3}{8},y+\frac{1}{2},y+\frac{3}{4}$	$\frac{5}{8},\bar{y},y+\frac{1}{4}$	no extra conditions
			$\bar{y}+\frac{1}{4},\frac{1}{8},y$	$\bar{y}+\frac{3}{4},\frac{7}{8},\bar{y}+\frac{1}{2}$	$y+\frac{3}{4},\frac{3}{8},y+\frac{1}{2}$	$y+\frac{1}{4},\frac{5}{8},\bar{y}$	
			$y,\bar{y}+\frac{1}{4},\frac{1}{8}$	$\bar{y}+\frac{1}{2},\bar{y}+\frac{3}{4},\frac{7}{8}$	$y+\frac{1}{2},y+\frac{3}{4},\frac{3}{8}$	$\bar{y},y+\frac{1}{4},\frac{5}{8}$	
			$\frac{1}{8},\bar{y}+\frac{1}{4},y$	$\frac{3}{8},y+\frac{3}{4},y+\frac{1}{2}$	$\frac{7}{8},\bar{y}+\frac{3}{4},\bar{y}+\frac{1}{2}$	$\frac{5}{8},y+\frac{1}{4},\bar{y}$	
			$y,\frac{1}{8},\bar{y}+\frac{1}{4}$	$y+\frac{1}{2},\frac{3}{8},y+\frac{3}{4}$	$\bar{y}+\frac{1}{2},\frac{7}{8},\bar{y}+\frac{3}{4}$	$\bar{y},\frac{5}{8},y+\frac{1}{4}$	
			$\bar{y}+\frac{1}{4},y,\frac{1}{8}$	$y+\frac{3}{4},y+\frac{1}{2},\frac{3}{8}$	$\bar{y}+\frac{3}{4},\bar{y}+\frac{1}{2},\frac{7}{8}$	$y+\frac{1}{4},\bar{y},\frac{5}{8}$	
96	g	. . m	x,x,z	$\bar{x},\bar{x}+\frac{1}{2},z+\frac{1}{2}$	$\bar{x}+\frac{1}{2},x+\frac{1}{2},\bar{z}$	$x+\frac{1}{2},\bar{x},\bar{z}+\frac{1}{2}$	no extra conditions
			z,x,x	$z+\frac{1}{2},\bar{x},\bar{x}+\frac{1}{2}$	$\bar{z},\bar{x}+\frac{1}{2},x+\frac{1}{2}$	$\bar{z}+\frac{1}{2},x+\frac{1}{2},\bar{x}$	
			x,z,x	$\bar{x}+\frac{1}{2},z+\frac{1}{2},\bar{x}$	$x+\frac{1}{2},\bar{z},\bar{x}+\frac{1}{2}$	$\bar{x},\bar{z}+\frac{1}{2},x+\frac{1}{2}$	
			$x+\frac{3}{4},x+\frac{1}{4},\bar{z}+\frac{3}{4}$	$\bar{x}+\frac{1}{4},\bar{x}+\frac{1}{4},\bar{z}+\frac{1}{4}$	$x+\frac{1}{4},\bar{x}+\frac{3}{4},z+\frac{3}{4}$	$\bar{x}+\frac{3}{4},x+\frac{3}{4},z+\frac{1}{4}$	
			$x+\frac{3}{4},z+\frac{1}{4},\bar{x}+\frac{3}{4}$	$\bar{x}+\frac{3}{4},z+\frac{3}{4},x+\frac{1}{4}$	$\bar{x}+\frac{1}{4},\bar{z}+\frac{1}{4},\bar{x}+\frac{1}{4}$	$x+\frac{1}{4},\bar{z}+\frac{3}{4},x+\frac{3}{4}$	
			$z+\frac{3}{4},x+\frac{1}{4},\bar{x}+\frac{3}{4}$	$z+\frac{1}{4},\bar{x}+\frac{3}{4},x+\frac{3}{4}$	$\bar{z}+\frac{3}{4},x+\frac{3}{4},x+\frac{1}{4}$	$\bar{z}+\frac{1}{4},\bar{x}+\frac{1}{4},\bar{x}+\frac{1}{4}$	
48	f	2 . mm	$x,0,0$	$\bar{x},\frac{1}{2},\frac{1}{2}$	$0,x,0$	$\frac{1}{2},\bar{x},\frac{1}{2}$	$0,0,x$	$\frac{1}{2},\frac{1}{2},\bar{x}$	hkl : $h=2n+1$
			$\frac{3}{4},x+\frac{1}{4},\frac{3}{4}$	$\frac{1}{4},\bar{x}+\frac{1}{4},\frac{1}{4}$	$x+\frac{3}{4},\frac{1}{4},\frac{1}{4}$	$\bar{x}+\frac{3}{4},\frac{3}{4},\frac{1}{4}$	$\frac{3}{4},\frac{1}{4},\bar{x}+\frac{3}{4}$	$\frac{1}{4},\frac{3}{4},x+\frac{3}{4}$	or $h+k+l=4n$
32	e	. 3 m	x,x,x	$\bar{x},\bar{x}+\frac{1}{2},x+\frac{1}{2}$					no extra conditions
			$\bar{x}+\frac{1}{2},x+\frac{1}{2},\bar{x}$	$x+\frac{1}{2},\bar{x},\bar{x}+\frac{1}{2}$					
			$x+\frac{3}{4},x+\frac{1}{4},\bar{x}+\frac{3}{4}$	$\bar{x}+\frac{1}{4},\bar{x}+\frac{1}{4},\bar{x}+\frac{1}{4}$					
			$x+\frac{1}{4},\bar{x}+\frac{3}{4},x+\frac{3}{4}$	$\bar{x}+\frac{3}{4},x+\frac{3}{4},x+\frac{1}{4}$					
16	d	. $\bar{3}$ m	$\frac{5}{8},\frac{5}{8},\frac{5}{8}$	$\frac{3}{8},\frac{7}{8},\frac{1}{8}$	$\frac{7}{8},\frac{1}{8},\frac{3}{8}$	$\frac{1}{8},\frac{3}{8},\frac{7}{8}$			hkl : $h=2n+1$
16	c	. $\bar{3}$ m	$\frac{1}{8},\frac{1}{8},\frac{1}{8}$	$\frac{7}{8},\frac{3}{8},\frac{5}{8}$	$\frac{3}{8},\frac{5}{8},\frac{7}{8}$	$\frac{5}{8},\frac{7}{8},\frac{3}{8}$			or $h,k,l=4n+2$ or $h,k,l=4n$
8	b	$\bar{4}$ 3 m	$\frac{1}{2},\frac{1}{2},\frac{1}{2}$	$\frac{1}{4},\frac{3}{4},\frac{1}{4}$					hkl : $h=2n+1$
8	a	$\bar{4}$ 3 m	$0,0,0$	$\frac{3}{4},\frac{1}{4},\frac{3}{4}$					or $h+k+l=4n$

Symmetry of special projections

Along [001] $p4mm$
$\mathbf{a}' = \frac{1}{4}(\mathbf{a}-\mathbf{b})$ $\mathbf{b}' = \frac{1}{4}(\mathbf{a}+\mathbf{b})$
Origin at $0,0,z$

Along [111] $p6mm$
$\mathbf{a}' = \frac{1}{6}(2\mathbf{a}-\mathbf{b}-\mathbf{c})$ $\mathbf{b}' = \frac{1}{6}(-\mathbf{a}+2\mathbf{b}-\mathbf{c})$
Origin at x,x,x

Along [110] $c2mm$
$\mathbf{a}' = \frac{1}{2}(-\mathbf{a}+\mathbf{b})$ $\mathbf{b}' = \mathbf{c}$
Origin at $x,x,\frac{1}{8}$

ORIGIN CHOICE 1

Maximal non-isomorphic subgroups

I
[2] $F\bar{4}3m$ (216) (1; 2; 3; 4; 5; 6; 7; 8; 9; 10; 11; 12; 37; 38; 39; 40; 41; 42; 43; 44; 45; 46; 47; 48)+
[2] $F4_132$ (210) (1; 2; 3; 4; 5; 6; 7; 8; 9; 10; 11; 12; 13; 14; 15; 16; 17; 18; 19; 20; 21; 22; 23; 24)+
[2] $Fd\bar{3}1$ ($Fd\bar{3}$, 203) (1; 2; 3; 4; 5; 6; 7; 8; 9; 10; 11; 12; 25; 26; 27; 28; 29; 30; 31; 32; 33; 34; 35; 36)+
[3] $F4_1/d12/m$ ($I4_1/amd$, 141) (1; 2; 3; 4; 13; 14; 15; 16; 25; 26; 27; 28; 37; 38; 39; 40)+
[3] $F4_1/d12/m$ ($I4_1/amd$, 141) (1; 2; 3; 4; 17; 18; 19; 20; 25; 26; 27; 28; 41; 42; 43; 44)+
[3] $F4_1/d12/m$ ($I4_1/amd$, 141) (1; 2; 3; 4; 21; 22; 23; 24; 25; 26; 27; 28; 45; 46; 47; 48)+
[4] $F1\bar{3}2/m$ ($R\bar{3}m$, 166) (1; 5; 9; 14; 19; 24; 25; 29; 33; 38; 43; 48)+
[4] $F1\bar{3}2/m$ ($R\bar{3}m$, 166) (1; 6; 12; 13; 18; 24; 25; 30; 36; 37; 42; 48)+
[4] $F1\bar{3}2/m$ ($R\bar{3}m$, 166) (1; 7; 10; 13; 19; 22; 25; 31; 34; 37; 43; 46)+
[4] $F1\bar{3}2/m$ ($R\bar{3}m$, 166) (1; 8; 11; 14; 18; 22; 25; 32; 35; 38; 42; 46)+

IIa none

IIb none

Maximal isomorphic subgroups of lowest index

IIc [27] $Fd\bar{3}m$ ($\mathbf{a}' = 3\mathbf{a}, \mathbf{b}' = 3\mathbf{b}, \mathbf{c}' = 3\mathbf{c}$) (227)

Minimal non-isomorphic supergroups

I none

II [2] $Pn\bar{3}m$ ($\mathbf{a}' = \frac{1}{2}\mathbf{a}, \mathbf{b}' = \frac{1}{2}\mathbf{b}, \mathbf{c}' = \frac{1}{2}\mathbf{c}$) (224)

Symmetry operations

For (0,0,0)+ set

(1) 1
(2) $2(0,0,\frac{1}{2})$ $0,\frac{1}{4},z$
(3) $2(0,\frac{1}{2},0)$ $\frac{1}{4},y,0$
(4) $2(\frac{1}{2},0,0)$ $x,0,\frac{1}{4}$
(5) 3^+ x,x,x
(6) $3^+(\frac{1}{3},-\frac{1}{3},\frac{1}{3})$ $\bar{x}+\frac{1}{6},x+\frac{1}{6},\bar{x}$
(7) $3^+(-\frac{1}{3},\frac{1}{3},\frac{1}{3})$ $x+\frac{1}{3},\bar{x}-\frac{1}{6},\bar{x}$
(8) $3^+(\frac{1}{3},\frac{1}{3},-\frac{1}{3})$ $\bar{x}+\frac{1}{6},\bar{x}+\frac{1}{3},x$
(9) 3^- x,x,x
(10) 3^- $x,\bar{x}+\frac{1}{2},\bar{x}$
(11) 3^- $\bar{x}+\frac{1}{2},\bar{x},x$
(12) 3^- $\bar{x}-\frac{1}{2},x+\frac{1}{2},\bar{x}$
(13) $2(\frac{1}{2},\frac{1}{2},0)$ $x,x-\frac{1}{4},\frac{3}{8}$
(14) 2 $x,\bar{x}+\frac{1}{4},\frac{1}{8}$
(15) $4^-(0,0,\frac{3}{4})$ $\frac{1}{2},\frac{1}{4},z$
(16) $4^+(0,0,\frac{1}{4})$ $0,\frac{3}{4},z$
(17) $4^-(\frac{3}{4},0,0)$ $x,\frac{1}{2},\frac{1}{4}$
(18) $2(0,\frac{1}{2},\frac{1}{2})$ $\frac{3}{8},y+\frac{1}{4},y$
(19) 2 $\frac{1}{8},y+\frac{1}{4},\bar{y}$
(20) $4^+(\frac{1}{4},0,0)$ $x,0,\frac{3}{4}$
(21) $4^+(0,\frac{1}{4},0)$ $\frac{3}{4},y,0$
(22) $2(\frac{1}{2},0,\frac{1}{2})$ $x-\frac{1}{4},\frac{3}{8},x$
(23) $4^-(0,\frac{3}{4},0)$ $\frac{1}{4},y,\frac{1}{2}$
(24) 2 $\bar{x}+\frac{1}{4},\frac{1}{8},x$
(25) $\bar{1}$ $\frac{1}{8},\frac{1}{8},\frac{1}{8}$
(26) $d(\frac{1}{4},\frac{3}{4},0)$ $x,y,\frac{3}{8}$
(27) $d(\frac{3}{4},0,\frac{1}{4})$ $x,\frac{3}{8},z$
(28) $d(0,\frac{1}{4},\frac{3}{4})$ $\frac{3}{8},y,z$
(29) $\bar{3}^+$ $x,x,x;$ $\frac{1}{8},\frac{1}{8},\frac{1}{8}$
(30) $\bar{3}^+$ $\bar{x}-1,x+1,\bar{x};$ $-\frac{1}{8},\frac{1}{8},\frac{7}{8}$
(31) $\bar{3}^+$ $x,\bar{x}+1,\bar{x};$ $\frac{1}{8},\frac{7}{8},-\frac{1}{8}$
(32) $\bar{3}^+$ $\bar{x}+1,x,x;$ $\frac{7}{8},-\frac{1}{8},\frac{1}{8}$
(33) $\bar{3}^-$ $x,x,x;$ $\frac{1}{8},\frac{1}{8},\frac{1}{8}$
(34) $\bar{3}^-$ $x+\frac{3}{2},\bar{x}-1,\bar{x};$ $\frac{5}{8},-\frac{1}{8},\frac{7}{8}$
(35) $\bar{3}^-$ $\bar{x}+\frac{1}{2},\bar{x}+\frac{3}{2},x;$ $-\frac{1}{8},\frac{7}{8},\frac{5}{8}$
(36) $\bar{3}^-$ $\bar{x}+1,x+\frac{1}{2},\bar{x};$ $\frac{7}{8},\frac{5}{8},-\frac{1}{8}$
(37) $g(\frac{1}{4},-\frac{1}{4},\frac{1}{2})$ $x+\frac{1}{4},\bar{x},z$
(38) m x,x,z
(39) $\bar{4}^-$ $-\frac{1}{4},\frac{1}{4},z;$ $-\frac{1}{4},\frac{1}{4},\frac{1}{4}$
(40) $\bar{4}^+$ $\frac{1}{2},0,z;$ $\frac{1}{2},0,0$
(41) $\bar{4}^-$ $x,-\frac{1}{4},\frac{1}{4};$ $\frac{1}{4},-\frac{1}{4},\frac{1}{4}$
(42) $g(\frac{1}{2},\frac{1}{4},-\frac{1}{4})$ $x,y+\frac{1}{4},\bar{y}$
(43) m x,y,y
(44) $\bar{4}^+$ $x,\frac{1}{2},0;$ $0,\frac{1}{2},0$
(45) $\bar{4}^+$ $0,y,\frac{1}{2};$ $0,0,\frac{1}{2}$
(46) $g(-\frac{1}{4},\frac{1}{2},\frac{1}{4})$ $\bar{x}+\frac{1}{4},y,x$
(47) $\bar{4}^-$ $\frac{1}{4},y,-\frac{1}{4};$ $\frac{1}{4},\frac{1}{4},-\frac{1}{4}$
(48) m x,y,x

For $(0,\frac{1}{2},\frac{1}{2})$+ set

(1) $t(0,\frac{1}{2},\frac{1}{2})$
(2) 2 $0,0,z$
(3) 2 $\frac{1}{4},y,\frac{1}{4}$
(4) $2(\frac{1}{2},0,0)$ $x,\frac{1}{4},0$
(5) $3^+(\frac{1}{3},\frac{1}{3},\frac{1}{3})$ $x-\frac{1}{3},x-\frac{1}{6},x$
(6) 3^+ $\bar{x}+\frac{1}{2},x,\bar{x}$
(7) 3^+ $x,\bar{x},\bar{x}$
(8) 3^+ $\bar{x}+\frac{1}{2},\bar{x}+\frac{1}{2},x$
(9) $3^-(\frac{1}{3},\frac{1}{3},\frac{1}{3})$ $x-\frac{1}{6},x+\frac{1}{6},x$
(10) 3^- $x+\frac{1}{2},\bar{x},\bar{x}$
(11) $3^-(\frac{1}{3},\frac{1}{3},-\frac{1}{3})$ $\bar{x}+\frac{1}{3},\bar{x}+\frac{1}{6},x$
(12) 3^- $\bar{x},x,\bar{x}$
(13) $2(\frac{3}{4},\frac{3}{4},0)$ $x,x,\frac{1}{8}$
(14) $2(-\frac{1}{4},\frac{1}{4},0)$ $x,\bar{x}+\frac{1}{2},\frac{3}{8}$
(15) $4^-(0,0,\frac{1}{4})$ $\frac{1}{4},0,z$
(16) $4^+(0,0,\frac{3}{4})$ $\frac{1}{4},\frac{1}{2},z$
(17) $4^-(\frac{3}{4},0,0)$ $x,\frac{1}{2},-\frac{1}{4}$
(18) $2(0,\frac{1}{2},\frac{1}{2})$ $\frac{3}{8},y-\frac{1}{4},y$
(19) 2 $\frac{1}{8},y+\frac{3}{4},\bar{y}$
(20) $4^+(\frac{1}{4},0,0)$ $x,0,\frac{1}{4}$
(21) $4^+(0,\frac{3}{4},0)$ $\frac{1}{2},y,-\frac{1}{4}$
(22) $2(\frac{1}{4},0,\frac{1}{4})$ $x,\frac{1}{8},x$
(23) $4^-(0,\frac{1}{4},0)$ $0,y,\frac{3}{4}$
(24) $2(-\frac{1}{4},0,\frac{1}{4})$ $\bar{x}+\frac{1}{2},\frac{3}{8},x$
(25) $\bar{1}$ $\frac{1}{8},\frac{3}{8},\frac{3}{8}$
(26) $d(\frac{1}{4},\frac{1}{4},0)$ $x,y,\frac{1}{8}$
(27) $d(\frac{3}{4},0,\frac{3}{4})$ $x,\frac{1}{8},z$
(28) $d(0,\frac{3}{4},\frac{1}{4})$ $\frac{3}{8},y,z$
(29) $\bar{3}^+$ $x,x+\frac{1}{2},x;$ $\frac{1}{8},\frac{5}{8},\frac{1}{8}$
(30) $\bar{3}^+$ $\bar{x}-1,x+\frac{3}{2},\bar{x};$ $-\frac{1}{8},\frac{5}{8},\frac{7}{8}$
(31) $\bar{3}^+$ $x,\bar{x}+\frac{1}{2},\bar{x};$ $\frac{1}{8},\frac{3}{8},-\frac{1}{8}$
(32) $\bar{3}^+$ $\bar{x}+1,\bar{x}-\frac{1}{2},x;$ $\frac{7}{8},-\frac{5}{8},\frac{1}{8}$
(33) $\bar{3}^-$ $x-\frac{1}{2},x-\frac{1}{2},x;$ $\frac{1}{8},\frac{1}{8},\frac{5}{8}$
(34) $\bar{3}^-$ $x+1,\bar{x}-\frac{3}{2},\bar{x};$ $\frac{1}{8},-\frac{5}{8},\frac{7}{8}$
(35) $\bar{3}^-$ $\bar{x},\bar{x}+1,x;$ $-\frac{1}{8},\frac{7}{8},\frac{1}{8}$
(36) $\bar{3}^-$ $\bar{x}+\frac{1}{2},x,\bar{x};$ $\frac{3}{8},\frac{1}{8},-\frac{1}{8}$
(37) m $x+\frac{1}{2},\bar{x},z$
(38) $g(\frac{1}{4},\frac{1}{4},\frac{1}{2})$ $x-\frac{1}{4},x,z$
(39) $\bar{4}^-$ $0,0,z;$ $0,0,0$
(40) $\bar{4}^+$ $\frac{1}{4},-\frac{1}{4},z;$ $\frac{1}{4},-\frac{1}{4},\frac{1}{4}$
(41) $\bar{4}^-$ $x,\frac{1}{4},\frac{1}{4};$ $\frac{1}{4},\frac{1}{4},\frac{1}{4}$
(42) $g(\frac{1}{2},-\frac{1}{4},\frac{1}{4})$ $x,y+\frac{1}{4},\bar{y}$
(43) $g(0,\frac{1}{2},\frac{1}{2})$ x,y,y
(44) $\bar{4}^+$ $x,0,0;$ $0,0,0$
(45) $\bar{4}^+$ $\frac{1}{4},y,\frac{1}{4};$ $\frac{1}{4},\frac{1}{4},\frac{1}{4}$
(46) m $\bar{x},y,x$
(47) $\bar{4}^-$ $\frac{1}{2},y,0;$ $\frac{1}{2},0,0$
(48) $g(\frac{1}{4},\frac{1}{2},\frac{1}{4})$ $x-\frac{1}{4},y,x$

For $(\frac{1}{2},0,\frac{1}{2})$+ set

(1) $t(\frac{1}{2},0,\frac{1}{2})$
(2) 2 $\frac{1}{4},\frac{1}{4},z$
(3) $2(0,\frac{1}{2},0)$ $0,y,\frac{1}{4}$
(4) 2 $x,0,0$
(5) $3^+(\frac{1}{3},\frac{1}{3},\frac{1}{3})$ $x+\frac{1}{2},x-\frac{1}{6},x$
(6) 3^+ $\bar{x},x,\bar{x}$
(7) 3^+ $x+\frac{1}{2},\bar{x},\bar{x}$
(8) 3^+ $\bar{x},\bar{x}+\frac{1}{2},x$
(9) $3^-(\frac{1}{3},\frac{1}{3},\frac{1}{3})$ $x-\frac{1}{6},x-\frac{1}{3},x$
(10) $3^-(-\frac{1}{3},\frac{1}{3},\frac{1}{3})$ $x+\frac{1}{6},\bar{x}+\frac{1}{6},\bar{x}$
(11) 3^- $\bar{x},\bar{x},x$
(12) 3^- $\bar{x},x+\frac{1}{2},\bar{x}$
(13) $2(\frac{1}{4},\frac{1}{4},0)$ $x,x,\frac{1}{8}$
(14) $2(\frac{1}{4},-\frac{1}{4},0)$ $x,\bar{x}+\frac{1}{2},\frac{3}{8}$
(15) $4^-(0,0,\frac{1}{4})$ $\frac{3}{4},0,z$
(16) $4^+(0,0,\frac{3}{4})$ $-\frac{1}{4},\frac{1}{2},z$
(17) $4^-(\frac{1}{4},0,0)$ $x,\frac{1}{4},0$
(18) $2(0,\frac{3}{4},\frac{3}{4})$ $\frac{1}{8},y,y$
(19) $2(0,-\frac{1}{4},\frac{1}{4})$ $\frac{3}{8},y+\frac{1}{2},\bar{y}$
(20) $4^+(\frac{3}{4},0,0)$ $x,\frac{1}{4},\frac{1}{2}$
(21) $4^+(0,\frac{1}{4},0)$ $\frac{1}{4},y,0$
(22) $2(\frac{1}{2},0,\frac{1}{2})$ $x+\frac{1}{4},\frac{3}{8},x$
(23) $4^-(0,\frac{3}{4},0)$ $-\frac{1}{4},y,\frac{1}{2}$
(24) 2 $\bar{x}+\frac{3}{4},\frac{1}{8},x$
(25) $\bar{1}$ $\frac{3}{8},\frac{1}{8},\frac{3}{8}$
(26) $d(\frac{3}{4},\frac{3}{4},0)$ $x,y,\frac{1}{8}$
(27) $d(\frac{1}{4},0,\frac{3}{4})$ $x,\frac{3}{8},z$
(28) $d(0,\frac{1}{4},\frac{1}{4})$ $\frac{1}{8},y,z$
(29) $\bar{3}^+$ $x-\frac{1}{2},x-\frac{1}{2},x;$ $\frac{1}{8},\frac{1}{8},\frac{5}{8}$
(30) $\bar{3}^+$ $\bar{x}-\frac{1}{2},x+\frac{1}{2},\bar{x};$ $-\frac{1}{8},\frac{1}{8},\frac{3}{8}$
(31) $\bar{3}^+$ $x-\frac{1}{2},\bar{x}+\frac{3}{2},\bar{x};$ $\frac{1}{8},\frac{7}{8},-\frac{5}{8}$
(32) $\bar{3}^+$ $\bar{x}+\frac{3}{2},\bar{x}+\frac{1}{2},x;$ $\frac{7}{8},-\frac{1}{8},\frac{5}{8}$
(33) $\bar{3}^-$ $x+\frac{1}{2},x,x;$ $\frac{5}{8},\frac{1}{8},\frac{1}{8}$
(34) $\bar{3}^-$ $x+1,\bar{x}-1,\bar{x};$ $\frac{1}{8},-\frac{1}{8},\frac{7}{8}$
(35) $\bar{3}^-$ $\bar{x},\bar{x}+\frac{1}{2},x;$ $-\frac{1}{8},\frac{3}{8},\frac{1}{8}$
(36) $\bar{3}^-$ $\bar{x}+\frac{3}{2},x-\frac{1}{2},\bar{x};$ $\frac{7}{8},\frac{1}{8},-\frac{5}{8}$
(37) m $x,\bar{x},z$
(38) $g(\frac{1}{4},\frac{1}{4},\frac{1}{2})$ $x+\frac{1}{4},x,z$
(39) $\bar{4}^-$ $0,\frac{1}{2},z;$ $0,\frac{1}{2},0$
(40) $\bar{4}^+$ $\frac{1}{4},\frac{1}{4},z;$ $\frac{1}{4},\frac{1}{4},\frac{1}{4}$
(41) $\bar{4}^-$ $x,0,0;$ $0,0,0$
(42) m $x,y+\frac{1}{2},\bar{y}$
(43) $g(\frac{1}{2},\frac{1}{4},\frac{1}{4})$ $x,y-\frac{1}{4},y$
(44) $\bar{4}^+$ $x,\frac{1}{4},-\frac{1}{4};$ $\frac{1}{4},\frac{1}{4},-\frac{1}{4}$
(45) $\bar{4}^+$ $0,y,0;$ $0,0,0$
(46) $g(\frac{1}{4},\frac{1}{2},-\frac{1}{4})$ $\bar{x}+\frac{1}{4},y,x$
(47) $\bar{4}^-$ $\frac{1}{4},y,\frac{1}{4};$ $\frac{1}{4},\frac{1}{4},\frac{1}{4}$
(48) $g(\frac{1}{2},0,\frac{1}{2})$ x,y,x

For $(\frac{1}{2},\frac{1}{2},0)$+ set

(1) $t(\frac{1}{2},\frac{1}{2},0)$
(2) $2(0,0,\frac{1}{2})$ $\frac{1}{4},0,z$
(3) 2 $0,y,0$
(4) 2 $x,\frac{1}{4},\frac{1}{4}$
(5) $3^+(\frac{1}{3},\frac{1}{3},\frac{1}{3})$ $x+\frac{1}{6},x+\frac{1}{3},x$
(6) 3^+ $\bar{x},x+\frac{1}{2},\bar{x}$
(7) 3^+ $x+\frac{1}{2},\bar{x}-\frac{1}{2},\bar{x}$
(8) 3^+ $\bar{x},\bar{x},x$
(9) $3^-(\frac{1}{3},\frac{1}{3},\frac{1}{3})$ $x-\frac{1}{3},x+\frac{1}{3},x$
(10) 3^- $x,\bar{x},\bar{x}$
(11) 3^- $\bar{x}+\frac{1}{2},\bar{x}+\frac{1}{2},x$
(12) $3^-(\frac{1}{3},-\frac{1}{3},\frac{1}{3})$ $\bar{x}-\frac{1}{3},x+\frac{1}{3},\bar{x}$
(13) $2(\frac{1}{2},\frac{1}{2},0)$ $x,x+\frac{1}{4},\frac{3}{8}$
(14) 2 $x,\bar{x}+\frac{3}{4},\frac{1}{8}$
(15) $4^-(0,0,\frac{3}{4})$ $\frac{1}{2},-\frac{1}{4},z$
(16) $4^+(0,0,\frac{1}{4})$ $0,\frac{1}{4},z$
(17) $4^-(\frac{1}{4},0,0)$ $x,\frac{3}{4},0$
(18) $2(0,\frac{1}{4},\frac{1}{4})$ $\frac{1}{8},y,y$
(19) $2(0,\frac{1}{4},-\frac{1}{4})$ $\frac{3}{8},y+\frac{1}{2},\bar{y}$
(20) $4^+(\frac{3}{4},0,0)$ $x,-\frac{1}{4},\frac{1}{2}$
(21) $4^+(0,\frac{3}{4},0)$ $\frac{1}{2},y,\frac{1}{4}$
(22) $2(\frac{3}{4},0,\frac{3}{4})$ $x,\frac{1}{8},x$
(23) $4^-(0,\frac{1}{4},0)$ $0,y,\frac{1}{4}$
(24) $2(\frac{1}{4},0,-\frac{1}{4})$ $\bar{x}+\frac{1}{2},\frac{3}{8},x$
(25) $\bar{1}$ $\frac{3}{8},\frac{3}{8},\frac{1}{8}$
(26) $d(\frac{3}{4},\frac{1}{4},0)$ $x,y,\frac{3}{8}$
(27) $d(\frac{1}{4},0,\frac{1}{4})$ $x,\frac{1}{8},z$
(28) $d(0,\frac{3}{4},\frac{3}{4})$ $\frac{1}{8},y,z$
(29) $\bar{3}^+$ $x+\frac{1}{2},x,x;$ $\frac{5}{8},\frac{1}{8},\frac{1}{8}$
(30) $\bar{3}^+$ $\bar{x}-\frac{3}{2},x+1,\bar{x};$ $-\frac{5}{8},\frac{1}{8},\frac{7}{8}$
(31) $\bar{3}^+$ $x+\frac{1}{2},\bar{x}+1,\bar{x};$ $\frac{5}{8},\frac{7}{8},-\frac{1}{8}$
(32) $\bar{3}^+$ $\bar{x}+\frac{1}{2},\bar{x},x;$ $\frac{3}{8},-\frac{1}{8},\frac{1}{8}$
(33) $\bar{3}^-$ $x,x+\frac{1}{2},x;$ $\frac{1}{8},\frac{5}{8},\frac{1}{8}$
(34) $\bar{3}^-$ $x+\frac{1}{2},\bar{x}-\frac{1}{2},\bar{x};$ $\frac{1}{8},-\frac{1}{8},\frac{3}{8}$
(35) $\bar{3}^-$ $\bar{x}-\frac{1}{2},\bar{x}+1,x;$ $-\frac{5}{8},\frac{7}{8},\frac{1}{8}$
(36) $\bar{3}^-$ $\bar{x}+1,x,\bar{x};$ $\frac{7}{8},\frac{1}{8},-\frac{1}{8}$
(37) $g(-\frac{1}{4},\frac{1}{4},\frac{1}{2})$ $x+\frac{1}{4},\bar{x},z$
(38) $g(\frac{1}{2},\frac{1}{2},0)$ x,x,z
(39) $\bar{4}^-$ $\frac{1}{4},\frac{1}{4},z;$ $\frac{1}{4},\frac{1}{4},\frac{1}{4}$
(40) $\bar{4}^+$ $0,0,z;$ $0,0,0$
(41) $\bar{4}^-$ $x,0,\frac{1}{2};$ $0,0,\frac{1}{2}$
(42) m $x,y,\bar{y}$
(43) $g(\frac{1}{2},\frac{1}{4},\frac{1}{4})$ $x,y+\frac{1}{4},y$
(44) $\bar{4}^+$ $x,\frac{1}{4},\frac{1}{4};$ $\frac{1}{4},\frac{1}{4},\frac{1}{4}$
(45) $\bar{4}^+$ $-\frac{1}{4},y,\frac{1}{4};$ $-\frac{1}{4},\frac{1}{4},\frac{1}{4}$
(46) m $\bar{x}+\frac{1}{2},y,x$
(47) $\bar{4}^-$ $0,y,0;$ $0,0,0$
(48) $g(\frac{1}{4},\frac{1}{2},\frac{1}{4})$ $x+\frac{1}{4},y,x$

International Tables for Crystallography (2006). Vol. A, Plane group 11, p. 102.

$p4mm$ $4mm$ Square

No. 11 $p4mm$ Patterson symmetry $p4mm$

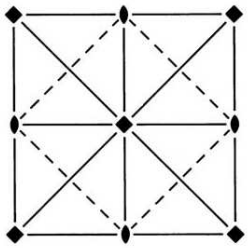

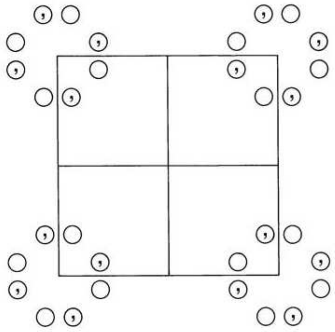

Origin at $4mm$

Asymmetric unit $0 \le x \le \frac{1}{2}; \quad 0 \le y \le \frac{1}{2}; \quad x \le y$

Symmetry operations

(1) 1	(2) 2 0,0	(3) 4^+ 0,0	(4) 4^- 0,0
(5) m 0,y	(6) m x,0	(7) m x,x	(8) m x,$\bar{x}$

Generators selected (1); $t(1,0)$; $t(0,1)$; (2); (3); (5)

Positions

Multiplicity, Wyckoff letter, Site symmetry			Coordinates				Reflection conditions
							General:
8	g	1	(1) x,y	(2) $\bar{x},\bar{y}$	(3) $\bar{y},x$	(4) $y,\bar{x}$	no conditions
			(5) $\bar{x},y$	(6) $x,\bar{y}$	(7) y,x	(8) $\bar{y},\bar{x}$	
							Special:
4	f	$..m$	x,x	$\bar{x},\bar{x}$	$\bar{x},x$	$x,\bar{x}$	no extra conditions
4	e	$.m.$	$x,\frac{1}{2}$	$\bar{x},\frac{1}{2}$	$\frac{1}{2},x$	$\frac{1}{2},\bar{x}$	no extra conditions
4	d	$.m.$	$x,0$	$\bar{x},0$	$0,x$	$0,\bar{x}$	no extra conditions
2	c	$2mm.$	$\frac{1}{2},0$	$0,\frac{1}{2}$			hk: $h+k=2n$
1	b	$4mm$	$\frac{1}{2},\frac{1}{2}$				no extra conditions
1	a	$4mm$	0,0				no extra conditions

Maximal non-isomorphic subgroups

I [2] $p411$ ($p4$, 10) 1; 2; 3; 4
[2] $p21m$ ($c2mm$, 9) 1; 2; 7; 8
[2] $p2m1$ ($p2mm$, 6) 1; 2; 5; 6

IIa none

IIb [2] $c4mg$ ($\mathbf{a}' = 2\mathbf{a}, \mathbf{b}' = 2\mathbf{b}$) ($p4gm$, 12)

Maximal isomorphic subgroups of lowest index

IIc [2] $c4mm$ ($\mathbf{a}' = 2\mathbf{a}, \mathbf{b}' = 2\mathbf{b}$) ($p4mm$, 11)

Minimal non-isomorphic supergroups

I none

II none

International Tables for Crystallography (2006). Vol. A, Plane group 17, pp. 108–109.

$p6mm$ $6mm$ Hexagonal

No. 17 $p6mm$ Patterson symmetry $p6mm$

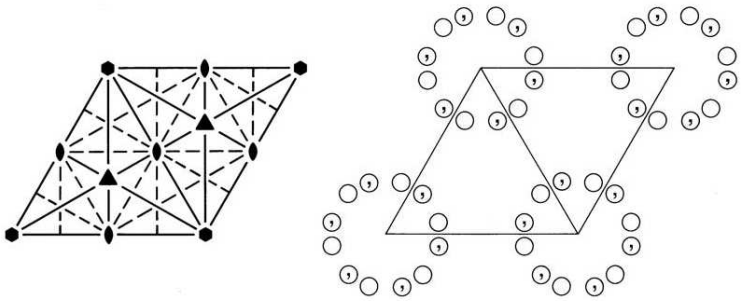

Origin at $6mm$

Asymmetric unit $0 \le x \le \frac{2}{3}$; $0 \le y \le \frac{1}{3}$; $x \le (1+y)/2$; $y \le x/2$

Vertices $0,0$ $\frac{1}{2},0$ $\frac{2}{3},\frac{1}{3}$

Symmetry operations

(1) 1	(2) 3^+ 0,0	(3) 3^- 0,0
(4) 2 0,0	(5) 6^- 0,0	(6) 6^+ 0,0
(7) m $x,\bar{x}$	(8) m $x,2x$	(9) m $2x,x$
(10) m x,x	(11) m $x,0$	(12) m $0,y$

Generators selected (1); $t(1,0)$; $t(0,1)$; (2); (4); (7)

Positions

Multiplicity, Wyckoff letter, Site symmetry			Coordinates			Reflection conditions
						General:
12	f	1	(1) x,y (4) $\bar{x},\bar{y}$ (7) $\bar{y},\bar{x}$ (10) y,x	(2) $\bar{y},x-y$ (5) $y,\bar{x}+y$ (8) $\bar{x}+y,y$ (11) $x-y,\bar{y}$	(3) $\bar{x}+y,\bar{x}$ (6) $x-y,x$ (9) $x,x-y$ (12) $\bar{x},\bar{x}+y$	no conditions
						Special: no extra conditions
6	e	. m .	$x,\bar{x}$	$x,2x$	$2\bar{x},\bar{x}$	$\bar{x},x$	$\bar{x},2\bar{x}$	$2x,x$
6	d	. . m	$x,0$	$0,x$	$\bar{x},\bar{x}$	$\bar{x},0$	$0,\bar{x}$	x,x
3	c	2 m m	$\frac{1}{2},0$	$0,\frac{1}{2}$	$\frac{1}{2},\frac{1}{2}$			
2	b	3 m .	$\frac{1}{3},\frac{2}{3}$	$\frac{2}{3},\frac{1}{3}$				
1	a	6 m m	$0,0$					

Maximal non-isomorphic subgroups

I
- [2] $p611$ ($p6$, 16) 1; 2; 3; 4; 5; 6
- [2] $p31m$ (15) 1; 2; 3; 10; 11; 12
- [2] $p3m1$ (14) 1; 2; 3; 7; 8; 9
- [3] $p2mm$ ($c2mm$, 9) 1; 4; 7; 10
- [3] $p2mm$ ($c2mm$, 9) 1; 4; 8; 11
- [3] $p2mm$ ($c2mm$, 9) 1; 4; 9; 12

IIa none

IIb none

Maximal isomorphic subgroups of lowest index

IIc [3] $h6mm$ ($\mathbf{a}'=3\mathbf{a},\mathbf{b}'=3\mathbf{b}$) ($p6mm$, 17)

Minimal non-isomorphic supergroups

I none

II none

$c2mm$ $2mm$ Rectangular

No. 9 $c2mm$ Patterson symmetry $c2mm$

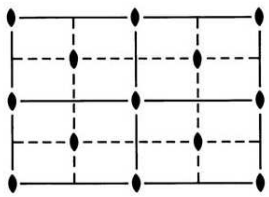

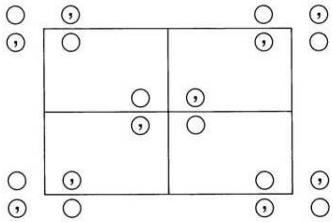

Origin at $2mm$

Asymmetric unit $0 \le x \le \frac{1}{4}$; $0 \le y \le \frac{1}{2}$

Symmetry operations

For $(0,0)+$ set

(1) 1 (2) 2 $0,0$ (3) m $0,y$ (4) m $x,0$

For $(\frac{1}{2},\frac{1}{2})+$ set

(1) $t(\frac{1}{2},\frac{1}{2})$ (2) 2 $\frac{1}{4},\frac{1}{4}$ (3) b $\frac{1}{4},y$ (4) a $x,\frac{1}{4}$

Generators selected (1); $t(1,0)$; $t(0,1)$; $t(\frac{1}{2},\frac{1}{2})$; (2); (3)

Positions

Multiplicity, Wyckoff letter, Site symmetry			Coordinates $(0,0)+$	Coordinates $(\frac{1}{2},\frac{1}{2})+$			Reflection conditions
							General:
8	f	1	(1) x,y	(2) $\bar{x},\bar{y}$	(3) $\bar{x},y$	(4) $x,\bar{y}$	hk: $h+k=2n$ $h0$: $h=2n$ $0k$: $k=2n$
							Special: as above, plus
4	e	$.m.$	$0,y$	$0,\bar{y}$			no extra conditions
4	d	$..m$	$x,0$	$\bar{x},0$			no extra conditions
4	c	$2..$	$\frac{1}{4},\frac{1}{4}$	$\frac{3}{4},\frac{1}{4}$			hk: $h=2n$
2	b	$2mm$	$0,\frac{1}{2}$				no extra conditions
2	a	$2mm$	$0,0$				no extra conditions

Maximal non-isomorphic subgroups

I	[2] $c1m1$ (cm, 5)	$(1;\ 3)+$
	[2] $c11m$ (cm, 5)	$(1;\ 4)+$
	[2] $c211$ ($p2$, 2)	$(1;\ 2)+$
IIa	[2] $p2gg$ (8)	$1;\ 2;\ (3;\ 4)+(\frac{1}{2},\frac{1}{2})$
	[2] $p2gm$ ($p2mg$, 7)	$1;\ 4;\ (2;\ 3)+(\frac{1}{2},\frac{1}{2})$
	[2] $p2mg$ (7)	$1;\ 3;\ (2;\ 4)+(\frac{1}{2},\frac{1}{2})$
	[2] $p2mm$ (6)	$1;\ 2;\ 3;\ 4$
IIb	none	

Maximal isomorphic subgroups of lowest index

IIc [3] $c2mm$ ($\mathbf{a}' = 3\mathbf{a}$ or $\mathbf{b}' = 3\mathbf{b}$) (9)

Minimal non-isomorphic supergroups

I [2] $p4mm$ (11); [2] $p4gm$ (12); [3] $p6mm$ (17)

II [2] $p2mm$ ($\mathbf{a}' = \frac{1}{2}\mathbf{a}, \mathbf{b}' = \frac{1}{2}\mathbf{b}$) (6)

Bibliography

[1] Hwang, J. et al. Biomimetics: forecasting the future of science, engineering, and medicine. Int J Nanomedicine. 2015; 10: 5701-5713

[2] Ravi, A. et al. Ecological Footprint Analysis- An Overview. AJER. 2013; 1: 12-19

[3] Cotteneir, S. Ab initio modelling for the design of TCO's structural properties. The future of transparent conducting oxides Seminar. Hasselt University, Martelareniaan 42 - B-3500, Hasselt. 26 Aug. 2014. Plenary Lecture.

[4] Yaghjian, A. Reflections on Maxwell's Treatise (Invited Paper). PIER. 2014; 149: 217

[5] Raabe, Dierk, Dr. Categories of Models. Computational Material Science: Modelling and Simulations in Material Science. New York: Wiley-VCH, 1998; 23-28. Print.

[6] Raabe, Dierk, Dr. Introduction. Computational Material Science: Modelling and Simulations in Material Science. New York: Wiley-VCH, 1998; 5-12. Print.

[7] Raabe, Dierk, Dr. Fundamentals. Computational Material Science: Modelling and Simulations in Material Science. New York: Wiley-VCH, 1998; 303-304. Print.

[8] Raabe, Dierk, Dr. Space and Time scales in Microstructure Simulations. Computational Material Science: Modelling and Simulations in Material Science. New York: Wiley-VCH, 1998; 305-307. Print.

[9] Theory and Modelling in Nanoscience Report. Workshop conducted at San Francisco by Basic Energy Sciences and Advanced Scientific Computing, Advisory Committees to the Office of Science, US Department of Energy. May 10-11,2002.

[10] Scanning Tunneling Microscope. IBM's 100 Icons of Progress. Reterieved from `http://www-03.ibm.com/ibm/history/ibm100/us/en/icons/`.

[11] Strohmaier, E. et al. The TOP500 List and Progress in High-Performance Computing. Computer. 2015; 48: 42-49, doi:10.1109/MC.2015.338

[12] Sholl, D.; Steckel, J. Density Functional Theory: A Practical Introduction; Wiley: 2011.

[13] Frenkel, D.; Smit, B. Understanding Molecular Simulation, 2nd ed.; Academic Press, Inc.: Orlando, FL, USA, 2001.

[14] Raabe, Dierk, Dr. Molecular Dynamics. Computational Material Science: Modelling and Simulations in Material Science. New York: Wiley-VCH, 1998; 87. Print.

[15] Evans, J. D. et al. Molecular Design of Amorphous Porous Organic Cages for Enhanced Gas Storage. J. Phys. Chem. C. 2015; 119: 7746-7754.

[16] Rappe, A. K. et al. A full periodic table force field for molecular mechanics and molecular dynamics simulations. J. Am. Chem. Soc. 1992; 114: 10024-10035.

[17] Cornell, W. D. et al. A Second Generation Force Field for the Simulation of Proteins, Nucleic Acids, and Organic Molecules. J. Am. Chem. Soc. 1995; 117: 5179-5197.

[18] Sun, H. COMPASS: An ab Initio Force-Field Optimized for Condensed-Phase Applications Overview with Details on Alkane and Benzene Compounds. J. Phys. Chem. B. 1998; 102: 7338-7364.

[19] Raabe, Dierk, Dr. Monte Carlo Simulation and Integration. Computational Material Science: Modelling and Simulations in Material Science. New York: Wiley-VCH, 1998; 61. Print.

[20] Raabe, Dierk, Dr. Simulation Techniques at the Micro-Meso Scale. Computational Material Science: Modelling and Simulations in Material Science. New York: Wiley-VCH, 1998; 111. Print.

[21] Foulkes, W. M. C. et al. Quantum Monte Carlo simulations of solids. Rev. Mod. Phys. 2001; 73: 33.

[22] VandeVondele, J. et al. Gaussian basis sets for accurate calculations on molecular systems in gas and condensed phases. J. Chem. Phys. 2007; 127: 114105.

[23] Corradini, D. et al. Carbon dioxide transport in molten calcium carbonate occurs through an oxo-Grotthuss mechanism via a pyrocarbonate anion. Nat. Chem. 2016; 8: 454-460.

[24] Curtarolo, S. et al. Predicting crystal structures with data mining of quantum calculations. Phys. Rev. Lett. 2003; 91: 135503.

[25] Nosengo N. The Material Code: Machine-learning techniques could revolutionize how materials science is done. Nature. 2016; 533: 22.

[26] A. Jain, et al. Commentary: The Materials Project: A materials genome approach to accelerating materials innovation. APL Mater. 2013; 1: 011002.

[27] Saal, J. et al. Materials design and discovery with high-throughput density functional theory: The open quantum materials database (OQMD). JOM. 2013; 65: 1501-1509.

[28] Landis, D.D. et al.The Computational Materials Repository. Comput. Sci. Eng. 2012; 14: 51.

[29] Curtarolo, S. et al. The high-throughput highway to computational materials design. Nat. Mater. 2013; 12: 191-201.

[30] Service, R.F. Materials scientists look to a data-intensive future. Science. 2012; 335: 1434-1435.

[31] Balachandran, P. V. et al. Identifying the 'inorganic gene' for high-temperature piezoelectric perovskites through statistical learning. Proc. R. Soc. A. 2011; 467: 2271-2290.

[32] Ulery, B.D. et al. Rational design of pathogen-mimicking amphiphilic materials as nanoadjuvants. Sci Rep. 2011; 1: 1980.

[33] Emery, A. A. et al. High-Throughput Computational Screening of Perovskites for Thermochemical Water Splitting Applications. Chem. Mater. 2016; 28: 5621-5634.

[34] Evans, J. D. et al. Computational Chemistry Methods for Nanoporous Materials. Chem. Mater., 2017; 29: 199.

[35] Jenkins, S.B. Nanoporous Materials: Types, Properties and Uses. New York: Nova Science Publishers, Inc.: 2010.

[36] Hollister P.; Harper T.E. The Nanotechnology Scientific Report, CMP Cientifica, 2002.

[37] Bell, A. T. The Impact of Nanoscience on Heterogeneous Catalysis. Science. 2003; 299: 1688-1691.

[38] Li, J.R. et al. Selective gas adsorption and separation in metal-organic frameworks. Chem. Soc. Rev. 2009; 38: 1477.

[39] Morris, R. E. et al. Gas Storage in Nanoporous Materials. Angew. Chem. Int. Ed. 2008; 47: 4966-4981.

[40] Della Rocca, J. D. et al. Nanoscale Metal-Organic Frameworks for Biomedical Imaging and Drug Delivery. Acc. Chem. Res. 2011; 44: 957-968.

[41] Zhang Q. et. al. ZnO Nanostructures for Dye-Sensitized Solar Cells. Advanced Materials. 2009; 21: 4087-4108.

[42] Simon P. et. al. Materials for electrochemical capacitors. Nature Materials. 2008; 7: 845-854.

[43] Furukawa, H. et al. The Chemistry and Applications of Metal-Organic Frameworks. Science. 2013; 341: 1230444-1230444.

[44] Haidary S. M. et al. Nanoporous Silicon as Drug Delivery Systems for Cancer Therapies. J Nanomaterials 2012; 2012: 1-15.

[45] Chakraborty M. et al. Quasi Monocrystalline Porous Silicon (QMPS)- A potential material for optoelectronic and photovoltaic applications. Nanoporous Materials: Types, Properties and Uses. New York: Nova Science Publishers, Inc. 2010; 261.

[46] Ott W. B. Introduction. Crystallography - An Introduction. Berlin: Springer., 2011; 1. Print.

[47] Hall S. and McMahon B. Genesis of the Crystallographic Information File/Historical Introduction. International Tables for Crystallography- Vol G Defination and Exchange of Crystallographic Data. Dordrecht: Springer., 2005; 2. Print.

[48] Glasser, L. Crystallographic Information Resources. J. Chem. Educ., 2016; 93 (3): 542-549.

[49] Crystallographic Open Database. Retrieved from `http://www.crystallography.net/cod/`.

[50] International Crystal Structure Database. Retrieved from `https://icsd.fiz-karlsruhe.de/`.

[51] The Materials Project. Retrieved from `https://materialsproject.org/`.

[52] Minerals by Name. Amethyst Galleries, Inc. Retrieved from `http://www.galleries.com/minerals_by_name`.

[53] Importing, adding, and exporting structures. QuantumWise. Retrieved from `http://docs.quantumwise.com/tutorials/builder_manual/builder_import/builder_import.html`.

[54] Hall S. and McMahon B. Specification of the Crystallographic Information File (CIF)/Concepts and Specifications. International Tables for Crystallography- Vol G Defination and Exchange of Crystallographic Data. Dordrecht: Springer., 2005; 20. Print.

[55] Hahn T. Space-group symbols and their use. International Tables for Crystallography- Vol A Space-Group Symmetry. Dordrecht: Springer., 2005; 817. Print.

[56] Ott W. B. Space groups. Crystallography - An Introduction. Berlin: Springer., 2011; 1. Print.

[57] Halite CIF file can be downloaded from COD. `svn://www.crystallography.net/cod/cif/9/00/85/9008566.cif`.

[58] Wondratschek H. Special topics on space groups. International Tables for Crystallography- Vol A Space-Group Symmetry. Dordrecht: Springer., 2005; 732. Print.

[59] Steps to retrieve information. `http://cryst.ehu.es/` >> Space-group symmetry >> WYCKPOS

[60] Software information can be retrieved from `http://jp-minerals.org/vesta/en/`.

[61] Steps to visualize crystal structure online. `http://cryst.ehu.es/` >> Structure Utilities >> VISUALIZE

[62] Stokes H. et al. FINDSYM: Program for Identifying the Space Group Symmetry of a Crystal. J. Appl. Cryst. 2005; 38: 237-238.

[63] CIF file can be uploaded on `http://stokes.byu.edu/iso/findsym.php`.

[64] Make CIF File Defining Crystal Structure. QuantumWise. Retrieved from `http://docs.quantumwise.com/tutorials/cif/cif.html`.

[65] Hahn T. Data listed in the space group tables/Symmetry of special projections/Contents and arrangement of the tables/Guide to the use of the space-group tables. International Tables for Crystallography-Vol A Space-Group Symmetry. Dordrecht: Springer., 2005; 33. Print.

[66] Download link for silicon CIF file. `www.crystallography.net/cod/cif/9/00/85/9008566.cif`.

[67] Hahn T. Space Group 227/The 230 Space groups. International Tables for Crystallography- Vol A Space-Group Symmetry. Dordrecht: Springer., 2006; 696. Print.

[68] Hahn T. Plane Group 11/The 17 Plane groups. International Tables for Crystallography- Vol A Space-Group Symmetry. Dordrecht: Springer., 2006; 102. Print.

[69] Hahn T. Plane Group 17/The 17 Plane groups. International Tables for Crystallography- Vol A Space-Group Symmetry. Dordrecht: Springer., 2006; 108. Print.

[70] Hahn T. Plane Group 9/The 17 Plane groups. International Tables for Crystallography- Vol A Space-Group Symmetry. Dordrecht: Springer., 2006; 100. Print.

[71] Ott W. B. Compound Symmetry Operations/Principles of Symmetry. Crystallography - An Introduction. Berlin: Springer., 2011; 69. Print.

[72] Hahn T. Projections of Symmetry elements/Symmetry of special projections/Contents and arrangement of the tables/Guide to the use of the space-group tables. International Tables for Crystallography- Vol A Space-Group Symmetry. Dordrecht: Springer., 2005; 33. Print.

[73] Ott W. B. The Stereographic Projection/Morphology. Crystallography - An Introduction. Berlin: Springer., 2011; 36. Print.

[74] Ott W. B. The Wulff Net/Morphology. Crystallography - An Introduction. Berlin: Springer., 2011; 40. Print.

[75] N0rskov, J. K. et al. Towards the computational design of solid catalysts. Nature Chemistry. 2009; 1: 37-46.

[76] Ouyang G. et al. Nanocavity: A novel functional nanostructural unit. Nanoporous Materials: Types, Properties and Uses. New York: Nova Science Publishers, Inc. 2010; 163.

[77] Ballufi, R. W. et al. Kinetics of Materials. New Jersey: John Wiley & Sons, Inc., 2005.

[78] Gilman, J. J. Direct measurements of the surface energies of crystals. Journal of Applied Physics. 1960; 31, 2208-2218.

[79] Metois, J. J. et al. Absolute surface energy determination. Surface Science 2004; 548, 13-21.

[80] Gilman, J. J. Surface and interfacial energies. Electronic Basis for the Strength of Materials. Cambridge: Cambridge University Press. 2003; 255.

[81] Ramamoorthy. et al. Defects on TiO2 (110) surfaces. Physical Review B. 1994; 49.23, 16721.

[82] Lang, N. D. et al. Theory of Metal Surfaces: Work Function. Physical Review B. 1971; 3.4, 1215.

[83] Hammer B. et al. Theoretical surface science and catalysis-calculations and concepts. Advances in catalysis. 2000; 45, 71.

[84] Norskov Jens K. et al. Density functional theory in surface chemistry and catalysis Proceedings of the National Academy of Sciences. 2011; 108.3, 937.

[85] Sun W. et al. Efficient creation and convergence of surface slabs. Surface Science. 2013; 617, 53-59.

[86] Tran R. et al. Surface energies of elemental crystals. Scientific Data. 2016; 3, 160080.

[87] Santoro A. et al. Determination of the Reduced Cells. Acta Cryst. A. 1970; 26, 124.

[88] Arnold H. Transformations of the coordinate system (unit-cell transformations)/Transformations in Crystallography. International Tables for Crystallography- Vol A Space-Group Symmetry. Dordrecht: Springer., 2006; 78. Print.

[89] Hohenberg P. et al. Inhomogeneous electron gas. Phys. Rev. 1964; 136, B864-B871.

[90] Kohn W. Self-consistent equations including exchange and correlation effects. Phys. Rev. 1965; 140, A1133-A1138.

[91] Kiejna A. et al., Comparison of the full-potential and frozencore approximation approaches to density-functional calculations of surfaces. Phys. Rev. B. 2006; 73, 035404.

[92] Hamann D. R. et al. Norm-conserving pseudopotentials. Phys. Rev. Lett. 1979, 43, 1494-1497.

[93] Kleinman L. et al. Efficacious form for model pseudopotentials. Phys. Rev. Lett. 1982; 48, 1425-1428.

[94] Vanderbilt D. et al. Soft self-consistent pseudopotentials in a generalized eigenvalue formalism. Phys. Rev. B. 1990; 41, 7892-7895.

[95] Blochl P. E. et al. Projector augmented-wave method. Phys. Rev. B. 1994; 50, 17953-17979.

[96] Slater J. C. et al. Wave functions in a periodic potential. Phys. Rev. 1937; 51, 846-851.

[97] Mattsson A.E. In pursuit of the "Divine" Functional. Science. 2002; 298, 759.

[98] Lejaeghere L. et al. Reproducibility in density functional theory calculations of solids. Science. 2016; 351, aad3000.

[99] Kresse, G. et al. Efficient iterative schemes for ab initio total-energy calculations using a plane-wave basis set. Phys. Rev. B. 1996; 54, 11169-11186.

[100] Giannozzi P. et al., J. Phys. Condens. Matter. 2009; 21, 395502. More information can retrieved from `http://www.quantum-espresso.org`.

[101] Perdew, J. et al. Generalized gradient approximation made simple. Physical review letters. 1996; 77, 3865-3868.

[102] Marzari N. et al. Maximally localized generalized Wannier functions for composite energy bands. Phys. Rev. B. 1997; 56, 12847.

[103] Johnson S. Block-iterative frequency-domain methods for Maxwell's equations in a planewave basis. Optics Express. 2001; 8, 173-190.

[104] Lindgren, S. A. et al. Low-energy electron diffraction from Cu(111): Subthreshold effect and energy-dependent inner potential; surface relaxation and metric distances between spectra. Physical Review B. 1984; 29.2, 576.

[105] Binnig G. et al. 77 reconstruction on Si(lll) resolved in real space. Physical Review Letters. 1983; 50, 120-123.

[106] Brommer K. et al. Ab initio theory of the Si(lll)-(7×7) surface reconstruction. Physical review letters. 1992; 68, 1355-1359.

[107] Jaccodine, R. J. Surface energy of germanium and silicon. Journal of The Electrochemical Society. 1963; 110, 524.

[108] Miller W. et al. Surface free energies of solid metals. Estimation from liquid surface tension measurements. Surface Science. 1977; 62, 267-276.

[109] Mills K. C. et al. Review of surface tension data for metallic elements and alloys: Part 1 - Pure metals. International Materials Reviews. 2016; 51, 329-351.

[110] Keene B. J. Review of data for the surface tension of pure metals. International Materials Reviews. 1993; 38, 157-192.

[111] Ooi N. et al. Density functional study of graphite bulk and surface properties. Carbon. 2006; 44, 231-242.

[112] Zhang J. M. et al. Missing row reconstruction on three low index surfaces often FCC metals. Crystal Research and Technology. 2009; 44, 275-280.

[113] Shen T. D. et al. Photoluminescence from mechanically milled Si and SiO2 spowders. Phys. Rev. B. 1997; 55, 7615.

[114] Guilinger T.R. Nondestructive Measurement of Porous Silicon Thickness Using X-Ray Reflectivity. J. Electrochem. Soc. 1995; 142, 1634.

[115] Canham L.T. Pore type, shape, size, volume and surface area in porous silicon/Porosity. Properties of Porous silicon. London: INSPEC, The Institution of Electrical Engineers. 1997; 83. Print.

[116] Kaushik, V.S. et al. Microstructure Of Pores In n^+ Silicon. Materials Letters. 1991; 1, 109.

[117] Unno H. et al. X-ray diffraction investigation of n-type porous silicon, J Electrochem. Soc. 1987; 134, 645.

[118] Sing K.S.W. et al. Reporting Physorption data for gas/solid systems. Pure Appl. Chem. 1985; 57, 603.

[119] Rouquerol J. et al. Recommendations for the characterization of porous solids. Pure Appl. Chem. 1994; 66, 1739-58.

[120] Hermann H. et al. Geometric models for isotropic random porous media: A review. Advances in material science and engineering. 2014; 2014, 562874.

[121] Jenkins, S.B. Preface. Nanoporous Materials: Types, Properties and Uses. New York: Nova Science Publishers, Inc.: 2010.

[122] Check Quantum Confinement topic on the Potential well page on Wikipedia. Retrieved from `https://en.wikipedia.org/wiki/Potential_well`

[123] Boccaletti S. et. al. The structure and dynamics of multilayer networks. Physics Reports. 2014; 544, 1-122.

[124] Barthelemy M. Spatial Networks. Physics Reports. 2011; 499, 1-101.

[125] Check other practical applications on the pdf. Retreived from `http://www.utdallas.edu/~besp/teaching/mst-applications.pdf`

[126] Kruskal J.B. On the shortest spanning subtree of a graph and the traveling salesman problem. Proc. Amer. Math. Soc. 1956; 7, 48-50.

[127] Prim R.C. Shortest Connection Networks And Some Generalizations. Bell Labs Technical Journal. 1957; 36, 1389-1401.

[128] Kasana H.S. et al. Minimum Spanning Tree algorithm/Network Analysis. Introductory Operations Research. Springer Inter. Edn. 2011: 5, 254. Print.

[129] Yao Z. et. al. Improved neighbor list algorithm in molecular simulations using cell decomposition and data sorting method. Computer Physics Communications. 2004; 161, 27-35.

[130] Humphrey W. et al. VMD - Visual Molecular Dynamics. J. Molec. Graphics, 1996; 14, 33-38.

[131] Squires TM. et. al. Microfluidics: Fluid physics at the nanoliter scale. Rev. Mod. Phys. 2005; 77, 977-1026.

[132] Albert R. Statistical mechanics of complex networks. Rev. Mod. Phys. 2002; 74, 47-97.

[133] Liu B. et. al. Comparative investigation of a newly optimized modified embedded atom method potential with other potentials for silicon. Computational Materials Science. 2015; 109, 277-286.

[134] Lee Y. et al. Quantifying similarity of pore geometry in naoporous materials. Nature Communications. 2017; 8, 15396.